Chemical Science

REVIEW

Check for updates

Disilane-bridged architectures: an emerging class of molecular materials

Zhikuan Zhou, [ID] *[a] Lizhi Gai, [ID] [a] Li-Wen Xu, [ID] [a] Zijian Guo [ID] [b] and Hua Lu [ID] *[a]

Disilanes are organosilicon compounds that contain saturated Si–Si bonds. The structural characteristics of Si–Si single bonds resemble those of C–C single bonds, but their electronic structure is more similar to that of C=C double bonds, as Si–Si bonds have a higher HOMO energy level. These organosilicon compounds feature unique intramolecular σ electron delocalization, low ionization potentials, polarizable electronic structure, and σ–π interaction. It has been demonstrated that the employment of disilane units (Si–Si) is a versatile and effective approach for finely adjusting the photophysical properties of organic materials in both solution and solid states. In this review, we present and discuss the structure, properties, and relationships of novel σ–π-conjugated hybrid architectures with saturated Si–Si σ bonds. The application of disilane-bridged σ-conjugated compounds as optoelectronic materials, multifunctional solid-state emitters, CPL, and non-linear optical and stimuli-responsive materials is also reviewed.

1. Introduction

Numerous studies exploring the chemistry of silicon, an element that is abundant on our planet, have yielded a plethora of important applications in modern chemistry and cutting-edge materials, with a particular emphasis on functional organosilicon compounds.[1–8] Using silicon atoms as bridges within the π-fused structures has emerged as an effective approach for creating unique materials with remarkable electronic and photophysical characteristics, which are typically challenging to attain using carbon-based π-components.[9–13] Among organosilicon compounds, disilanes that contain saturated Si–Si bonds have been studied for over 80 years.[14–18] The σ-bonds in saturated Si–Si compounds are highly stable thermally and nonpolarized. They are conformationally similar to C–C single bonds but have longer bond lengths of 2.64 Å, a lower dissociation energy of 220–300 kJ mol^{-1}, and a lower torsional barrier of 1.0 kcal mol^{-1}.[19] Besides, the electrons involved in the Si–Si σ bond exhibit a striking ability to delocalize throughout the silicon skeleton, resembling the behavior of electrons in a π-conjugated system.[20,21] This distinctive phenomenon of σ-electron delocalization is referred to as σ-conjugation.[22] Interestingly, the highest occupied molecular orbital (HOMO) energy level of a Si–Si σ bond is comparable to that of a C=C π-orbital due to the inherent electropositivity of

silicon;[23] thus a Si–Si single bond electronically behaves like a C=C double bond and can be conjugated with π systems to construct sophisticated σ–π hybrid architectures.

Introducing Si–Si bonds into π-conjugated structures provides an approach to adjust their electrochemical and photophysical characteristics, and bring novel functionality to organic materials through the phenomenon of σ–π conjugation.[24] From an electronic perspective, efficient σ–π conjugation between σ-orbitals of the Si–Si bond and π-orbitals of the adjacent covalently linked aryl groups[25] can manipulate the functionality subtly (Fig. 1a).[26] What can't be ignored is that from a conformational aspect, the tetrahedral silicon and the bulky and flexible Si–Si unit are preferable for improving the solubility and reducing intermolecular interactions.[27] Thus, the Si–Si σ bond is crucial for the formation of stimuli-responsive soft crystalline materials.[28] Additionally, the silicon atom's lipophilicity makes them more effective in crossing membranes and increasing their biocompatibility.[29] The disilane bridge tends to deliver enhanced fluorescence, high solubility, and crystallinity to the hybrid molecules. Therefore, disilane-based molecular materials provide endless possibilities for applications in various frontier fields.

Disilane-bridged molecules are emerging as cutting-edge functional organic materials.[30] In light of the surging research on disilane-bridged molecular materials, this review focuses on the recent progress of structures, optical properties, and applications of organic small molecules containing disilane units (Fig. 1b). We introduce the general design of σ-conjugated molecules as high performance multifunctional organic materials. The aim is to give in-depth insight into the unique molecular properties brought by a silane chain, and the relationship of material functions with molecular structures.

[a]Key Laboratory of Organosilicon Chemistry and Material Technology, Ministry of Education, Key Laboratory of Organosilicon Material Technology of Zhejiang Province, College of Material Chemistry and Chemical Engineering, Hangzhou Normal University, 2318 Yuhangtang Road, Hangzhou 311121, China. E-mail: zkzhou@hznu.edu.cn; hualu@hznu.edu.cn

[b]State Key Laboratory of Coordination Chemistry, School of Chemistry and Chemical Engineering, Chemistry and Biomedicine Innovation Center (ChemBIC), Nanjing University, 163 Xianlin Avenue, Nanjing 210023, China
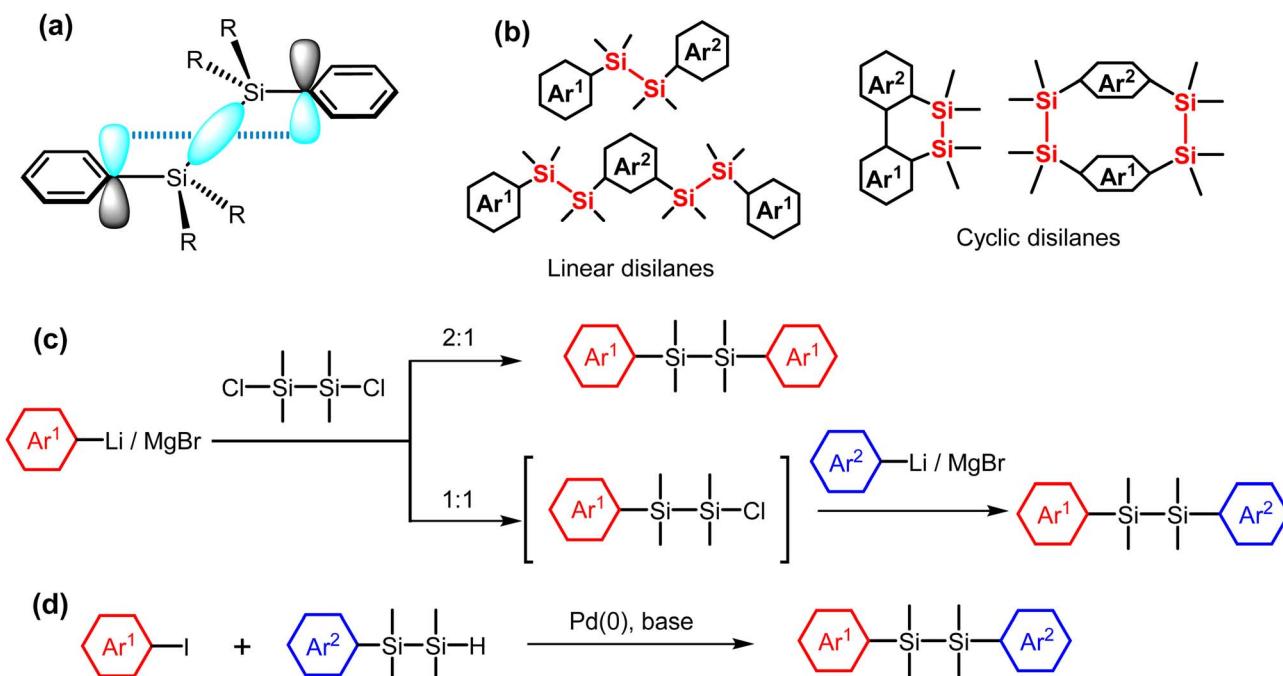
Fig. 1 (a) Schematic representation of σ−π conjugation in aryldisilane. (b) The scope of this review. (c) Salt elimination reaction to synthesize disilane-bridged architectures. (d) Pd-catalyzed cross-coupling reaction.

2. General synthetic methods of disilane-bridged systems

Si–Si bonds are generally stable to construct complex σ–π hybrid molecules. The commonly used synthetic approaches for the design of disilane-based molecules are salt elimination and Pd-catalyzed Si–C coupling (Fig. 1c and d). A salt elimination reaction refers to the reaction of chlorosilane with the Grignard or organolithium reagent, which has been widely used for almost a century-long time.[31] The starting materials are easily accessible and the products can have symmetrical and unsymmetrical structures. However, when preparing structurally unsymmetrical molecules, there are usually byproducts with symmetrical structures, and the yield and selectivity of the products are unsatisfactory. The most challenging aspect of this method is that aryl units with nucleophilic functional groups are incompatible with the strongly active organometallic reagents. This disadvantage limits the construction of well-defined disilane-bridged architectures with diverse functionalities.[32]

In the past three decades, the silylation of aryl halides with hydrosilanes catalyzed by transition metals has emerged as a prevalent method for synthesizing functional silanes.[33] In 1997, Masuda *et al.* reported the first example of palladium(0)-catalyzed silylation of aryl halides with hydrosilane.[34] Following this, several groups continued to develop a variety of synthetically advantageous methods for the palladium/rhodium-catalyzed silylation of arenes.[35–42] Despite several advantages of this method, such as mild reaction conditions and good functional group tolerance, the silylation of aryl iodides with hydrodisilanes was believed to be a rather tough and intricate task due to the susceptibility of Si–Si bond cleavage in the presence of transition metal complexes.[2,43,44] Interestingly, in 2010, Yamanoi and Nishihara reported a pioneering approach for the silylation of arenes with tris(trimethylsilyl)silane or hydrodisilane catalyzed by Pd(P(*t*Bu)$_3$)$_2$ to afford hypersilylated or disilylated aromatic products without observation of Si–Si bond cleavage.[45] Notably, this method can tolerate a diverse range of functional groups, including trifluoromethyl, amino, hydroxyl, cyano, acetyl, and ester, thus providing efficient access to novel scaffolds containing Si–Si units. This method greatly enriched this class of compounds.

Beyond the above methods, a few reports have demonstrated the feasibility of using electrochemistry for the synthesis of disilanes since the late 1970s.[46–48] However, these methods rely on using dangerous electrode materials and can only produce disilanes with alkyl substitutions. At present, it is not possible to obtain disilanes with precisely defined structures incorporating organic chromophores as building blocks.

3. Disilane-bridged chromophores

3.1. Symmetric silane-bridged molecules

From a synthetic point of view, structurally symmetric diaryldisilanes are easier to prepare.[49] As a distinctive characteristic of Si–Si σ bonds, the photophysical properties of the σ–π conjugated system are significantly dependent on the molecular conformation, specifically the angles of torsion between the Si–Si σ-bond and the plane of the aromatic ring ($\omega1$) and rotation around the Si–Si bond ($\omega2$, Fig. 2).[25] The absorption spectrum of aryldisilanes is a composite of the absorption spectra of

different conformers present in the mixture, each with its own population. Therefore, the conformation–property relationship is one of the most important topics when investigating the photophysical properties of aryldisilanes.

Due to the low ionization potentials of the Si–Si bond, it behaves like an electron-donating chromophore with UV absorption at around 200 nm.[50] The HOMO energy level of Si–Si is in close proximity to that of the phenyl group, and thus, there is a strong σ–π interaction in aryldisilanes with simply substituted phenyl as the end-capping group. However, in aryldisilanes with polycyclic aromatic hydrocarbons or other large π-conjugated chromophores as the end-capping groups, the difference between the HOMO energy level of Si–Si and the large π systems is relatively larger. Hence, in addition to the σ–π conjugation effect, the photophysical properties of these σ–π hybrids depend more on the intramolecular interaction between the two end-capping aromatic groups.

Diphenyldisilanes **1–3** were employed as model compounds to study the conformationally dependent intramolecular interactions (Fig. 2).[51] In compounds **2** and **3**, butyl chains were utilized to manually control the torsion angles ω1 and ω2 of disilane units. ω1 is considered as a measure of the degree of σ–π conjugation. 90° would be the ideal degree for the most effective σ–π conjugation.[25] ω2 mainly affects the stability of

disilane compounds, and the preferred torsional angles are 180° (anti, A) and 60° (gauche, G).[52] These two isomers cannot interconvert. The UV absorption maxima of the *trans* isomer **3** slightly redshifted by 4 nm compared to that of the *cis* isomer **2**, indicating a larger ω1 being beneficial for effective σ–π conjugation.[25] These results demonstrate that the conformationally dependent σ–π conjugation interaction can be effectively controlled through the conformation constraint.[53]

Compounds **1**, **4**, and **5** are used to study the intra- and intermolecular forces that enable molecules to exist stably in the solid and gaseous states. The conformational flexibility of the disilane unit is highly advantageous for studying multiple interacting forces.[54] Terminal aryl groups with variable electron-accepting strength were employed to examine aryl–aryl stacking interactions in the gas phase and in the solid state through gas electron diffraction (GED). The pentafluorophenyl and penta-chlorophenyl substituents are strong enough to force the molecules to aggregate in the solid and gaseous states, while unsubstituted phenyl cannot achieve this. London dispersion forces contribute increasingly along the series **1** < **4** < **5**. Among the three compounds, **5** has the most intense intramolecular interactions due to the pentachlorophenyl groups. Despite the significant distortion of the Si–C₆Cl₅ units, the *syn* conformation is the only one present in both gaseous and solid states.
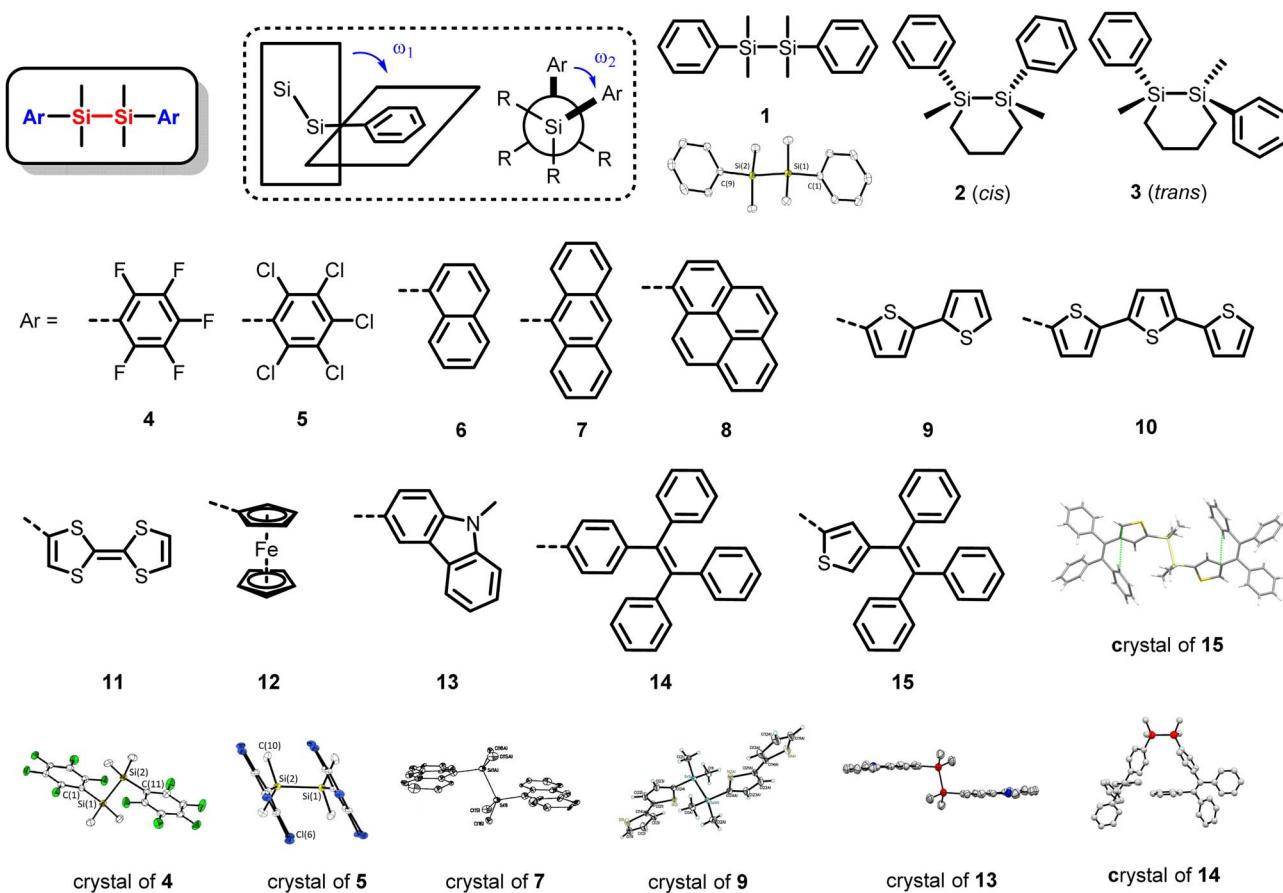
Fig. 2 Symmetrical diaryldisilanes and partial crystal structures. Reproduced with permission from ref. 54, Copyright 2020, Wiley-VCH, from ref. 56, Copyright 2003, American Chemical Society, from ref. 57, Copyright 2018, Royal Society of Chemistry, from ref. 61, Copyright 2020, American Chemical Society, from ref. 26, Copyright 2020, Chinese Chemical Society, from ref. 63, Copyright 2022, Royal Society of Chemistry.

These results demonstrate that $\omega 2$ is largely dependent on the interaction between terminal aryl groups.

Polycyclic aromatic hydrocarbon units such as anthryl, naphthyl, and pyrenyl groups are different from the phenyl group in that they readily form excimers in the excited state. In compounds 6–8, naphthyl, anthryl, and pyrenyl groups were linked through disilane chains to elucidate the effect of excimer/exciplex formations and multiple intramolecular interactions on the photophysical properties.[55,56] These compounds exhibit a combination of π–π interactions between two aromatic groups and σ–π interactions between the phenyl group and the silicon chain unit. 6, and 7 were found to exhibit the strongest excimer fluorescence, which is different from their carbon chain bridged analogues. Si–Si to aryl group σ–π^* charge-transfer (CT) fluorescence was observed in longer silane chain bridged compounds. This interaction enhanced the photostability of arylsilanes under UV irradiation.

Thienyl substituents are commonly recognized as electron donors, and are frequently employed as electron reservoirs in π-type carbon-based materials with a donor–acceptor (D–A) structure. Oligothienyl catenated disilanes 9, and 10 were synthesized.[57] The nearly perpendicular Si–Si–C–C_{Th} torsion angle (92°) in 9 suggests that there is a nearly perfect σ–π conjugation between the Si–Si bond and the adjacent thiophene fragments. Furthermore, the main UV absorption band of this compound is noticeably red-shifted in comparison to that of simple aryl derivatives. In solution, compound 9 exhibits emission spectra with intramolecular charge transfer (ICT) character, while compound 10 displays both ICT and locally excited (LE) bands. Photoluminescence quantum yields (PLQYs) of 9, and 10 in DCM are 0.26, and 0.17, respectively.

A disilane unit was also employed as a spacer to connect electronically active moieties to build model compounds for investigating intramolecular electron transfer. In symmetric disilane bridged bis-tetrathiafulvalenes (TTFs) 11,[58] no electronic interaction was detected between the two TTF units. However, in metallocene systems 12,[59] electronic coupling via both through-bond and through-space interactions may play a crucial role when these systems are linked by saturated bridges.[60] Two distinctive reversible redox processes were observed. In MeOH, the Si–Si bond underwent cleavage to yield the methoxysilane derivatives upon photolysis. Other optoelectronic functional organic chromophores were also employed as terminal units in aryldisilanes. Carbazole end-capped molecule 13 was reported.[61] It retained most of the emission color of carbazole; however, it showed high solubility in common organic solvents, high thermostability, and enhanced emission efficacy in the solid states ($\Phi_F = 0.33$). It may have found potential application as deep-blue organic emitters.[62]

Recently, a series of disilane bridged bis-TPE (tetraphenylethylene) 14 and bis-TPT (triphenylvinylthiophene) 15 were developed by us to study the electronic and conformational effect of a silane chain on the photophysical properties of aggregation induced emission (AIE) luminogens.[26,63] The absorption spectrum profiles of 14 and 15 were found to be the same as that of terminal TPE and TPT, indicating that disilane possesses excellent ability to maintain the original color. This is beneficial for constructing transparent functional molecular materials. Compound 14 exhibited a distorted conformation in its crystal structure, whereas compound 15 adopted an extended all-trans configuration with both end aryl groups parallel to each other (Fig. 2). The intermolecular interaction of TPE and TPT was further inhibited by the silane chain and the emission PLQYs of 14 and 15 in the solid state were 0.39 and 0.61, respectively.

The electron-donating nature, σ-conjugation and the flexibility of an oligosilane chain presents new opportunities for fabricating σ–π hybrid models for analyzing the photophysical process in charge-transfer. Acceptor–donor–acceptor (ADA) model compound 17 featuring an electron-deficient cyanovinyl-substituted arene (A) on either side of a permethylated hexasilane core (D) was reported, which exhibits distinct charge carrier mobilities compared with its alkane chain bridged analogues 16.[64] The unusual gauche conformation in the single crystal structure of 17 causes the σ-conjugation axis to face the π plane of an adjacent molecule, which is believed to enhance charge transport.[65] The electronic structure of the hybrid materials (16 and 17) is significantly influenced by the presence of silicon. In compound 16, the HOMO and the lowest unoccupied molecular orbital (LUMO) are situated on separate aromatic rings and exhibit no orbital density on the alkane chain. In contrast, in gauche-17, the HOMO is spread across the silane chain, while the LUMO is localized on a single aromatic ring (Fig. 3a). Additionally, the hybrid material's crystalline films deposited via solution showed a noteworthy enhancement in mobility for space charge limited current (SCLC), up to 100-fold higher than reported in the literature for photoinduced hole transport in films made of oligosilanes. The results of steady state and ultrafast spectroscopic measurements indicate that the charge separation (CS) process is asymmetric, which means that it occurs directly after light absorption.[66] Femtosecond stimulated Raman spectroscopy (FSRS) was employed to investigate the process of ICT in a system following photoexcitation. The results confirmed that the photoexcitation causes ICT from the electron-rich silane unit to the electron-poor cyano(ester)vinyl group, as evidenced by the similarity between the Raman spectrum of the excited silane and that of a reduced acceptor unit. The observed asymmetric ICT is attributed to the symmetry breaking of the excited state, which is influenced by the conformation of the central Si chain. Furthermore, the degree of charge separation was found to increase with the length of the silane chain.

Recently, a new series of ADA organosilanes 18–19 has been developed.[67] In these linear oligosilanes, disilane and tetrasilane chains were used to control the electron-donating ability; meanwhile, terminal groups with variable electron-accepting strength were employed. All the studied compounds have similar photoinduced ultrafast spectral dynamics, which involve the relaxation of the excited state with CS, and subsequent return to the ground state through charge recombination (CR). The rate of CR is dependent on the electron-accepting strength, which governs the intensity of the electronic coupling. Acceptors with weaker strength tend to have a larger
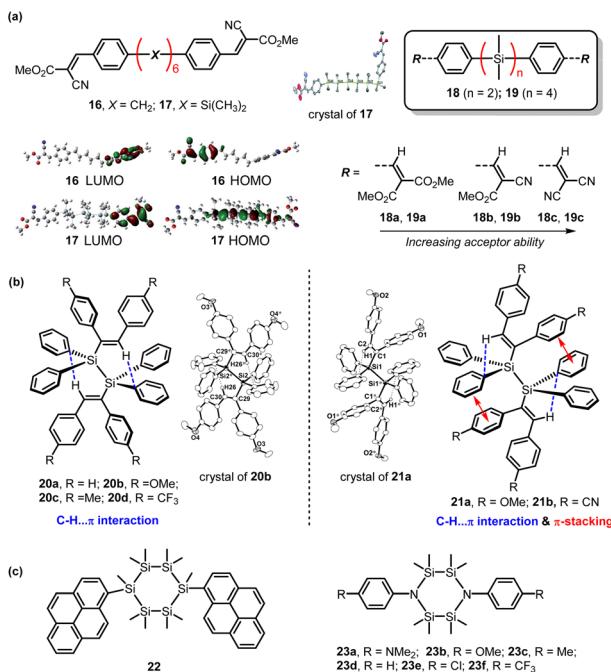
Fig. 3 (a) ADA type cyanovinylsilanes and their carbon analogues. Reproduced with permission from ref. 64, Copyright 2015, Royal Society of Chemistry. (b) Chemical and crystal structures of perphenylated disilanes. Reproduced with permission from ref. 69, Copyright 2012, American Chemical Society. (c) Structures of cyclohexasilanes and N-arylcyclosilazanes.

electronic coupling, resulting in rapid recombination, whereas stronger or moderately strong acceptors generate charge-separated states that are more stable and have a longer lifespan.

The photophysical properties of silane-bridged compounds in the solid state are highly influenced by the type of organic substituents they possess (specifically, their σ–π conjugation) and the molecular geometry. In aryldisilanes, the substituents on silicon atoms not only have an effect on the frontier molecular orbitals but also control the conformation and intramolecular interaction of the parent silanes. Until now, the most reported aryldisilane compounds employ peralkylated disilanes as linkage units since they are easy to synthesize and energetically stable. Aryl substituted disilane bridged compounds are rarely reported although they should exhibit different properties compared to peralkylated disilanes. Geometric isomers of perphenylated disilanes 20–21 were obtained indirectly through the reactions of diarylacetylenes with a dinickel complex bearing bridged silyl ligands.[68,69] Their X-ray crystallography conformations were classified into two types depending on the substituents on terminal phenyl groups. Compounds with substituents of H, Me, and CF$_3$ adopt a structure as 20b, which involves a C–H···π interaction between the vinylic C–H groups and the aryl group bonded to a different Si atom. Compounds with substituents of the strong electron accepting group CN adopt a structure as 21a, which has an intramolecular C–H···π interaction and π–π stacking between an aryl group of the C=C double bond and the phenyl ring bonded to Si atoms. Interestingly, a compound with an OMe

substituent exhibits the structures of two distinct molecules that are independent of each other within the unit cell as determined by crystallography. All compounds exhibited a fluorescence maximum at 393–488 nm in the solid state. The phenyl groups on the silicon atoms serve to promote proximity between the terminal chromophores, thereby facilitating interactions such as electron and/or energy transfer in the excited state. These interactions are responsible for the exceptional emission properties of the compound.

cis-1,4-Disubstituted cyclohexasilane 22 [70] was reported and the cyclohexasilane ring adopts a boat-like conformation in the crystal structure. Subsequently, a family of N-arylcyclosilazanes 23 were designed.[71] The cyclosilazane molecule exhibits a twist boat geometry, wherein the two nitrogen atoms are positioned in a trigonal planar conformation. The terminal substituent systematically perturbs HOMO energies. It can be inferred that the cyclosilazane rings have varying degrees of electron richness in comparison to a six-membered all-silicon ring.

3.2. Disilane-bridged donor–acceptor chromophores

The unique properties of a Si–Si bond prompted the design of novel disilane-bridged donor–acceptor molecules as an architecture for the creation of nonlinear optical materials. The Si–Si bridge may reduce but not fully cancel ICT between D and A moieties owing to σ conjugation, σ–π interaction, and low electronic polarizable energy. Early in the 1990s, a series of substituted diphenyldisilane and diphenylhexasilane 24,[72] 25,[73] 26 [74] having a dicyanovinyl acceptor and various donors have been synthesized via a salt elimination reaction. As for compounds 24c and 25, the optical first-order hyper-polarizability β increases 1.7 times with an elongated Si chain. The β value of compound 25 exceeds the maximum value reported for p-nitroaniline in methanol by 1.6 times. This is a good example for generating transparent material with excellent nonlinear properties. As for disilane-bridged compounds, the β values increased with the increasing donor strength (26 < 24a < 24b < 24c).

More than 20 years later, a set of disilane-bridged donor–acceptor architectures 27–32 were synthesized through Pd-catalyzed arylation of hydrosilanes and aryl iodides.[75] The electron donating substituents are p-N,N-dimethylamino, methoxyl and phenoxyl, while the electron-withdrawing substituents are carbethoxy and o-/m-/p-cyano. Both linear and non-linear optical properties were investigated in detail. The compounds displayed a purple-blue luminescence with an emission wavelength range of 360–420 nm and exhibited high quantum yields with a maximum PLQY of 0.81 (32b) in their solid state.

The crystal structure of 27a suggests that the two aryl groups are oriented in a parallel manner (Fig. 4a). The crystal structure of 28 is asymmetric due to steric hindrance. As a result, the compound exhibits a significant dipole moment between the donor and acceptor groups. Density functional theory (DFT) calculations unveiled that the luminescence behavior of the compound is influenced significantly by both LE states and ICT excited states.
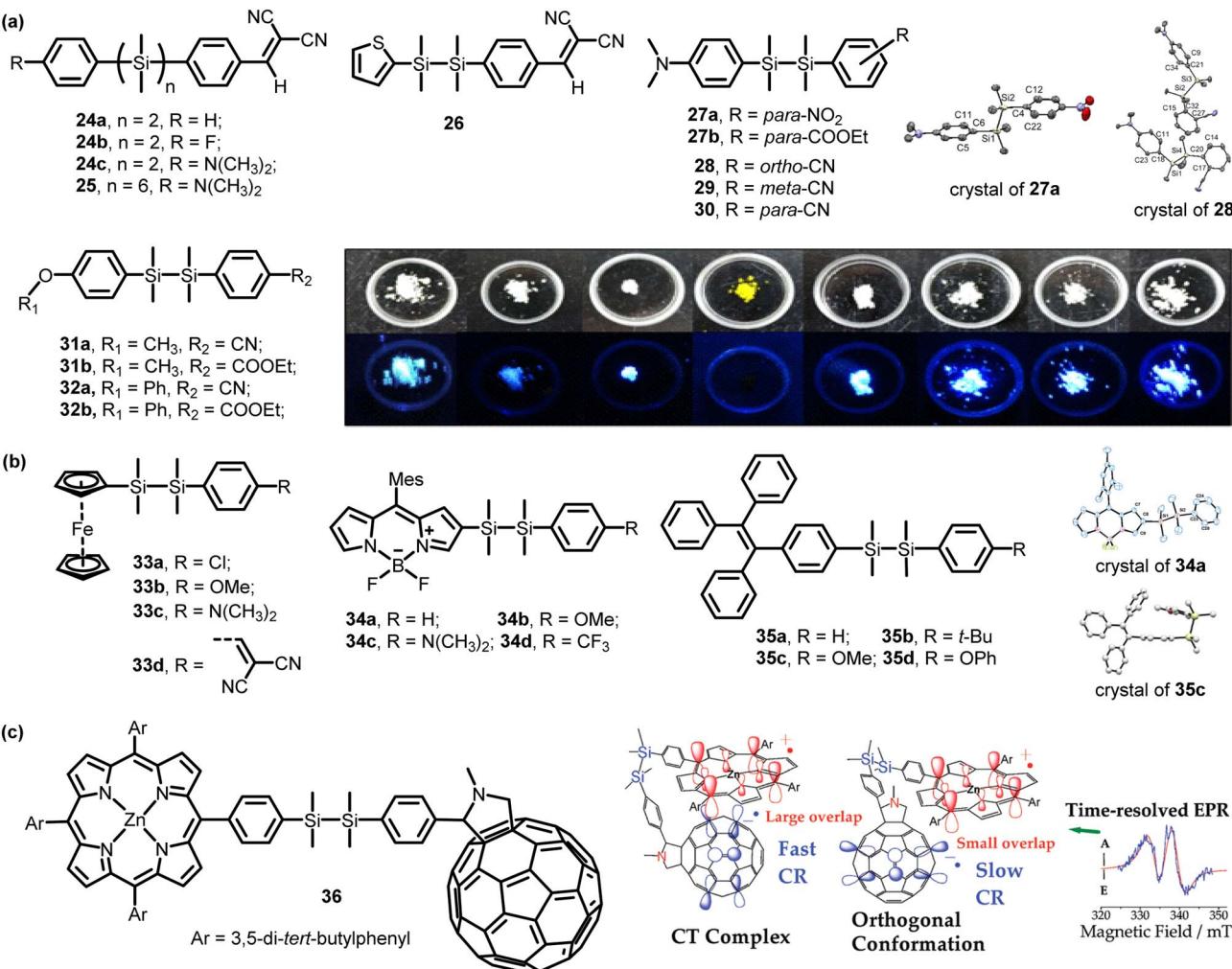
Fig. 4 (a) Molecular structures of the unsymmetrical 1,2-diaryldisilane derivatives containing various electron-donating and -withdrawing groups. Photographs showing appearance and emission colors of **27–32** in daylight and under 365 nm UV light. Reproduced with permission from ref. 75, Copyright 2015, American Chemical Society. (b) D–A structures contain ferrocenyl, TPE donors and BODIPY acceptors. Reproduced with permission from ref. 77, Copyright 2018, Royal Society of Chemistry, from ref. 78, Copyright 2021, Royal Society of Chemistry. (c) Structures and the time-resolved EPR spectrum of disilane bridged zinc porphyrin-fullerene molecules. Reproduced with permission from ref. 82, Copyright 2009, American Chemical Society.

The above pioneering studies have focused on the unique photoluminescence, electroluminescence and nonlinear optical properties of the D–σ–A system using a small π system as terminal units. Disilane-bridged D–σ–A architectures based on larger π conjugated chromophores were investigated recently. A redox active ferrocenyl group was used as a donor in disilane-bridged D–A structures (Fig. 4b).[76] The redox potentials of the Fe center are mildly affected by the different aryl substituents. For instance, replacing the most electron-donating substituent (NMe₂) with the most electron-withdrawing substituent (CH=C(CN)₂) leads to a shift in oxidation potential by 30 mV. The hyperpolarizabilities of complexes **33b** and **33c** closely resemble those of their corresponding substituted benzenes, except for compounds **33a** and **33d**, which contain the most electron-withdrawing substituents (*p*-Cl and *p*-CH=C(CN)₂).

A series of disilane-bridged boron dipyrrolmethane (BODIPY)-based D–σ–A architectures were reported by us, in which a BODIPY core was employed as the electron acceptor unit (Fig. 4b).[77] The σ–π conjugation between σ-orbitals of the Si–Si bond and π-orbitals of BODIPY slightly extend electron delocalization and result in 15–31 nm red-shifts in absorption compared with the precursor BODIPY core. Crystals of compounds **34a** revealed a rather folded conformation.

Subsequently, our group designed several disilane-bridged compounds **35** consisting of TPE (Fig. 4b).[78] Spectroscopic analysis revealed that these compounds showed the same absorption profiles as that of TPE with less than 8 nm redshift; thus, they are highly optically transparent. In the structure of **35c**, the angles of torsion between the Si–Si σ-bond axis and the plane of phenyl rings are 65.87 and 84.21°, implying that the σ-π conjugation is highly effective. Loose molecular packing caused by multiple intermolecular CH–π interactions and the steric-hindrance effect of Si may be attributed to the relatively lower PLQY of **35c** in the solid state compared with that of **35d**.

By virtue of the increased polarizability of the Si backbone and σ–π conjugation, these compounds exhibited strong reverse saturable absorbance (RSA) responses when doped in poly(bisphenol A carbonate) (PBC) thin films.

Porphyrin–fullerene dyads have been extensively researched and have demonstrated intricate photochemistry that is highly sensitive to the environment.[79] Their ability to achieve charge separation *via* photoinduced intramolecular electron transfer processes makes them a highly promising candidate for use in photovoltaic and photocatalytic applications.[80] Oligosilanes possess unique σ electron delocalization properties, making them highly suitable for studying complex photophysical processes within molecules. For example, D–A structures of zinc porphyrin (ZnP)–fullerenes utilizing oligosilane chains (silicon number $n = 1$–5) as bridges were synthesized.[81] The attenuation factor of electron transfer was evaluated based on the Si bridge length-dependent CS rate, and it was found to be 0.16 Å^{-1}. This value is consistent with those observed for other bridges that are σ-conjugated carbon-based units. In further study, a specific folded geometry of disilane-linked porphyrin–fullerene dyad **36** as well as its electronic properties were characterized (Fig. 4c).[82,83] In the photoinduced CS state of the folded molecule, the singly occupied molecular orbitals (SOMOs) are found to be mutually orthogonal. This orbital conformation prevents the energy-wasting CR despite ZnP and C_{60} being in close contact. The conformation of the tetrasilane linkers has little effect on the lifetimes of the CS states, and the degree of σ-conjugation has minimal impact on the CR rate.[84] These are markedly different from the π-conjugated linkers, where ET rates are unequivocally dependent on the nature of the linker. This disparity is one of the distinguishing features of silicon linkages.

Advanced stimuli responsive materials have raised significant concerns regarding the use of donor–acceptor–donor luminophores. A series of disilane-bridged D–A–D and A–D–A molecules were synthesized through Pd-catalyzed arylation of monohydrodisilane precursors with aryl diiodides.[85] The molecules exhibited broad UV/vis absorption bands attributed to both ICT and π–π* transitions upon excitation. In the solid state, all compounds showed moderate to strong fluorescence with a Φ_F up to 0.85 (**37a**). This was due to the efficient inhibition of intermolecular interactions, along with the suppression of non-radiative relaxation pathways and the photoinduced electron transfer (PET) effect.

Compounds **37d–37f**, and **38d–38f** contain triarylamine derivatives as donor units and benzothiazole or thienopyrazine as electron withdrawing groups.[86] In the solid state, their emission peaked at wavelengths between 485 and 547 nm, while in solution the maximum emission was observed at 480–670 nm. The compounds showed high fluorescence efficiency, with quantum yields (Φ_F) as high as 0.25 for compound **38d**. The single-crystal X-ray diffraction analysis of **37e** revealed that the suppression of intermolecular π–π interactions resulted in strong emission in the solid state and hindered the intramolecular rotation of the donor and acceptor units. These findings indicate that the intense emission observed in the solid state is attributed to the aggregation-induced emission

enhancement (AIEE) effect. **37g** and **38g** exhibit dual emissions in all solvents tested.[87] They also exhibited solid-state fluorescence and mechanochromic luminescence. The single-crystal X-ray analysis of **37h** revealed a butterfly-quasi-equatorial conformation, which is responsible for its unique emission properties (Fig. 5b).[88]

BODIPY-based D–σ–A–σ–D architectures **39** exhibit interesting dual fluorescence.[77] Typically, taking **39b** as an example, two separate absorption bands were observed at 523 nm and 556 nm in toluene. One can assign the fluorescence at 523 nm to either the BODIPY core or to the LE state with π π* character, which is not significantly affected by the solvent or substituents. In contrast, the fluorescence at 556 nm is attributed to the CT excited state, which is strongly influenced by both solvent and substituent effects. Two other π–σ–π–σ–π compounds **40** (ref. 57) and **41** (ref. 78) were reported during the research on D–σ–A compounds. The π units in these molecules are all electron-donating chromophores, and thus, no obvious ICT effect was observed in spectroscopic measurement. The PLQYs of **40** in DCM and **41** in the solid state are 0.76 and 0.92, respectively, both of which are higher than that of all their unsymmetrical D–σ–A analogs **9** and **34** under the same conditions.

3.3. Macrocyclic compounds incorporated with a disilane bridge

[2.2]paracyclophane and phanes based on it have been prepared, and their structures, reactions and applications have been investigated in detail since 1949.[89,90] Replacement of the C–C bridges of phanes by Si–Si is of particular interest in chemistry because the extensive mixing of σ–π orbitals results in through-bond conjugation and longer Si–Si bonds lead to more strain to phanes.[91] The first tetrasila[2.2]paracyclophane **42** was reported in 1986 by Sakurai using the synthetic method of Grignard reagent.[92] Tetrasila[2.2]paracyclophane displayed a σ(Si–Si)–π ICT band at 231 nm, and a smaller bending angle of the phenyl ring of 4.3° and a larger distance of 3.46 A° between phenyl rings than that of [2.2]paracyclophane (Fig. 6a). In the last three decades, various kinds of phanes with Si–Si bridges were reported,[91,93] and most were synthesized using organometallic reagents with low yields. The relationship between structures and UV absorption was investigated thoroughly *via* spectral measurement and DFT calculations. However, efficient methods to access unsymmetrical disilane-bridged cyclophane are challenging. Meanwhile, almost no luminescent properties in the solid state and applications were reported for these interesting phanes.

In 2017, Nishihara's group reported a series of tetrasila[2,2] cyclophane **42–51** through Pd-catalyzed dehalosilylation (Fig. 6b).[94] Notably, this method is particularly useful for diversity and functionalization of unsymmetrical Si–Si bridged cyclophanes, which are reported for the first time. Interestingly, these donor–acceptor molecules featuring a spatially separated HOMO and LUMO have potential for application as multifunctional fluorescent materials. Unsymmetrical tetrasila[2.2]-cyclophanes **45–51** exhibited blue-green emission arising from ICT. A flipping motion between *syn* and *anti* conformations was
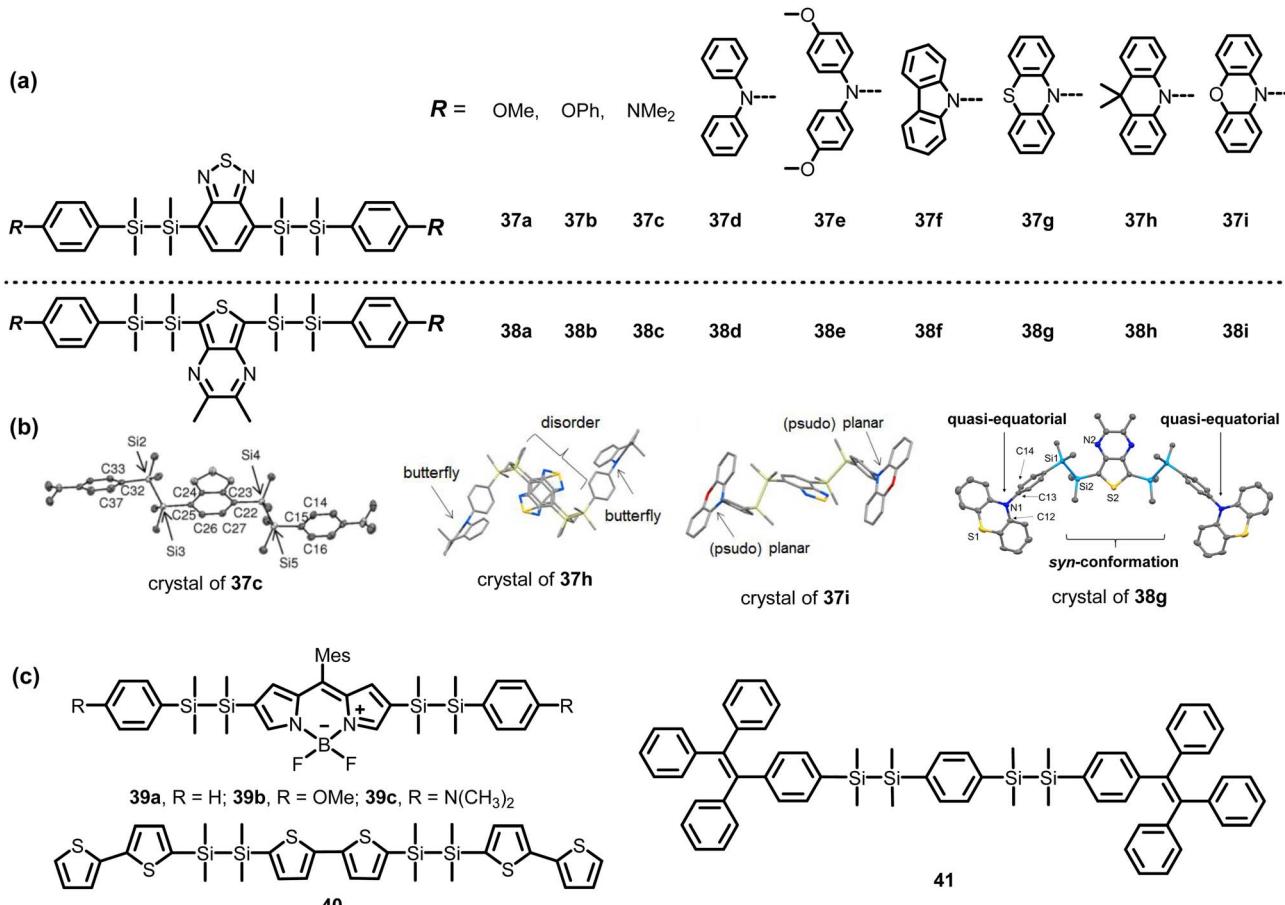
Fig. 5 (a) Molecular structures of disilane-bridged D–A–D and A–D–A compounds. (b) Single crystal structures of partial disilane-bridged D–A–D compounds. Reproduced with permission from ref. 85, Copyright 2016, Wiley-VCH, from ref. 88, Copyright 2022, American Chemical Society, from ref. 87, Copyright 2021, Wiley-VCH. (c) Molecular structures of disilane-bridged π–σ–π–σ–π compounds.

observed for compound **43**; this conformational mobility can be restricted by the macrocycle host molecules.

Polycyclic aromatic hydrocarbons bridged by disilane linkages were also reported. In 2010, Isobe developed a disilanyl double-pillared bisanthracene **52** as an OLED carrier transport material using a similar synthetic method reported by Sakurai.[95,96] Compound **53** is the isolated *syn* conformer of **52**. Disilanyl linkers can modulate structure and electrical properties for bipolar materials using a balanced combination of π and σ systems, which enables delocalization of charge and spin of radical ions throughout the whole molecule. Subsequently, they extend the substrate using tricyclic heteroarenes to form Si–Si bridged bisheteroarenes **54–56**,[97,98] and their fluctuating structure between anti and syn conformers in solution was observed due to the uniqueness of longer Si–Si bonds, which may contribute to special molecular devices with dynamic structures. Inspired by the hole transport of disilanyl double-pillared bisanthracene, the same group developed silacyclophane using naphthylene to form Si–Si bridged bisternaphthyl **57**,[99] which displayed interfused packing structures with a novel π-stack motif and herringbone. The unique packing mode made the structure rigid and recorded a moderate ability of hole transport. The use of 1,2-dichlorodisilane in the silylation of

β,β-dilithiated Ni(II)-porphyrin resulted in the formation of Ni(II)-porphyrin dimer **58**, which features double β-to-β disilane bridging.[100] Spectral analysis and DFT calculations revealed the weak yet distinct interporphyrinic interaction through σ–π conjugation.

Strained metallocenophanes furnishing an oligosilane chain offer a convenient route to organometallic polymers that consist of alternating organosilicon and π-conjugated units through ring-opening polymerization (ROP).[101] Besides, these metallocenophanes are highly intriguing due to their potential for exploring reactivity, including alkene insertions and Si–Si bond cleavage *via* transition metal catalysts.[102] Compared with a monosilane bridge, oligosilane bridges may release ring strain to metallocenophanes (Fig. 7a). Substituted ferrocenes **59** and **61a** with intramolecular disilane and trisilane bridges were first synthesized in 1972 by Kumada *et al.* through a salt metathesis reaction.[103] No spectroscopic and electrochemical properties were reported then. Subsequent electrochemical investigations of compounds **59** and **61a** revealed partially reversible behavior on the timescale of cyclic voltammetry for the former, while the latter showed complete reversibility.[60] In contrast to carbon-bridged ferrocenophanes, where a two-carbon bridge cannot withstand the distortions that occur upon oxidation and no
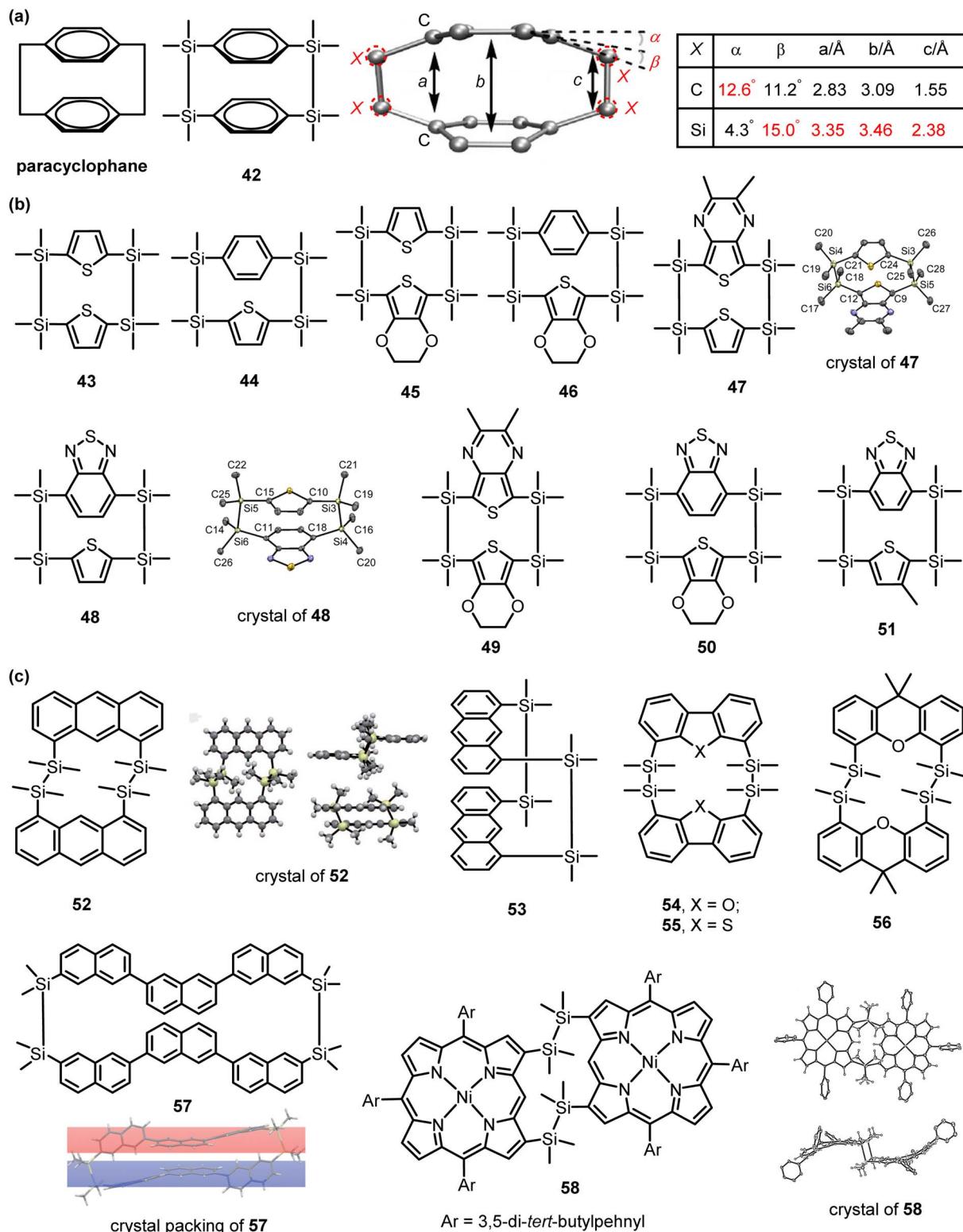
Fig. 6 (a) Chemical structures and crystal structures of [2.2]paracyclophanes bridged by ethylene and disilane. Reproduced with permission from ref. 90, Copyright 2020, Wiley-VCH. The data in the table are summarized from ref. 92. The structures of disilane bridged paracyclophane are composed of (b) simple aromatic hydrocarbons and (c) polycyclic aromatic hydrocarbons. Reproduced with permission from ref. 94, Copyright 2017, American Chemical Society, from ref. 95, Copyright 2010, Wiley-VCH, from ref. 99, Copyright 2014, Wiley-VCH, from ref. 100, Copyright 2015, Wiley-VCH.
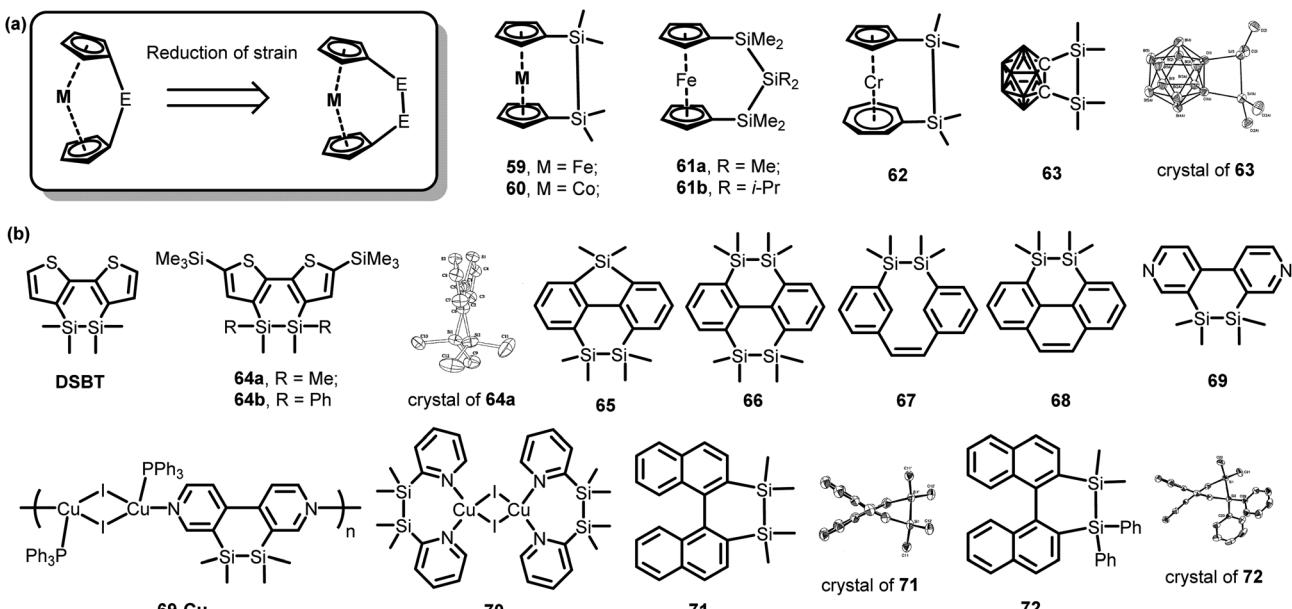
Fig. 7 (a) The structures of metallocenophanes containing a silane chain and the illustration of bond angles in metallocenophanes. Reproduced with permission from ref. 108, Copyright 1999, American Chemical Society. (b) Other cyclic compounds with intramolecular Si–Si bridges. Reproduced with permission from ref. 110, Copyright 1999, American Chemical Society, from ref. 115, Copyright 2000, American Chemical Society.

reversibility is observed, the results obtained from these compounds show a different behavior. The increased reversibility observed for **59** can be attributed to the longer bridging distance provided by the disilyl group.[104] Unexpectedly, its asymmetric unit contains four crystallographically independent molecules which are rotamers and distinctly different from each other conformationally. The projections of Newton-type structures along the central Si–Si bonds exhibit diverse conformations, which span from completely eclipsed to differing degrees of *gauche*. With an elongated silane chain, trisilane bridged complex **61b** adopted a nonstrained conformation.[105]

The center transition metals and the Si number of the silane chain play significant roles in controlling the ring strain, which is a key factor affecting the reactivity and cleavage of the Si–C(*ipso* carbon) bond. Regarding compound **59**, where an iron center is present with a d^6 configuration, all the occupied molecular orbitals mainly composed of d orbitals exhibit binding properties. On the other hand, compound **60** has a d^7 cobalt center, and the additional electron occupies a molecular orbital with significant antibonding character, leading to a decrease in the strength of the M-C_5H_4 bond. This effect has been reported for the derivative containing a hydrocarbon bridge.[106] Among the disilane bridged compounds, cyclopentadienyl–cycloheptatrienyl–chromium complex **62** (ref. 107) exhibits the least ring strain with a tilt angle of 2.6°. In disilane-bridged *o*-carborane **63**,[108] the Si–C(carborane)–C(carborane) bond angle is 99.0°, less than the ideal angle of 121.7°, which demonstrated its symmetric and strained conformation. Unlike its organic counterpart *o*-(disilanyl)-phenylene, the reaction of **63** with ethanol results in the breaking of a Si–C bond instead of

a Si–Si bond. Like other cyclic disilanes, when a solution of **63** is exposed to oxygen, an oxygen atom is inserted into the Si–Si bond.

Disilanobithiophene (DSBT) that bears an intramolecular Si–Si bridge was employed as a donor for designing donor–acceptor polymers.[109] The efficient conjugation along the polymer chains is suggested by the red-shifted UV-vis absorption of the polymers. TiO₂ electrodes were modified by using DSBT–pyrazine alternating polymers and were subsequently used in dye-sensitized solar cells. The highest power conversion efficiency of 0.89% was achieved. Dithienosilole derivatives **64a** and **64b** (ref. 110) adopted twisted bithiophene units with angles of 20.2° for **64a** and 24.6° for *trans*-**64b** between two thiophene rings. Despite the small twisting angles, these compounds maintain a high level of planarity. In triple-layer-type electroluminescent (EL) devices, **64b** displays remarkable electron-transporting capabilities.

The absorption spectra of silafluorene **65** with a disilane moiety were found to red-shift by 90 nm compared with that of silafluorene with a monosilane bridge,[111] indicating that the introduction of a Si–Si bond at the 4,5-positions of 9-silafluorenes can expand the conjugation system *via* σ–π (σ*–π*) conjugation. Large Stokes shifts of more than 220 nm were observed for **65**, which means substantial structural variations between the ground and excited states. The energy level of the HOMO, which was concentrated on the biphenyl unit and the Si–Si σ bond, was increased, while that of the LUMO, which was distributed over the biphenyl unit and the Si atoms but not the Si–Si σ bond, was decreased accordingly. Synthesis of other disilane-bridged biphenyls **66**,[111] and **67–68**(ref. 112) was also reported without property investigation.

The UV-vis absorption and photoluminescence bands of disilane-bridged bipyridyl **69** blue-shifted compared with that of monosilane-bridged bipyridyl, probably due to the more twisted bipyridyl units.[113] Complex polymer **69-Cu** exhibited phosphorescent properties. The more flexible and distant disilane bridge induces a moderate degree of twisting in the bipyridyl systems, thereby reducing the propensity to form aggregates in the solid state. The OLED devices that were constructed using **69-Cu** emitted yellow light, and their emission peak was at around 600 nm, while the maximum luminance that they achieved was120 cd m^{-2}. Dinuclear Cu complex **70** was prepared by using disilanylene bridged bispyridine ligands.[114] Analysis using single-crystal X-ray diffraction demonstrated that the size of the disilane linker moiety hindered the intermolecular $\pi\cdots\pi$ interaction. The complex displayed yellow-green phosphorescence with an emission band at 519 nm, PLQY of 0.60 and lifetime of 11 μs in the solid state.

The above mentioned disilane-bridged cyclic compounds exhibited weak to moderate intramolecular ring strain. In 2000, highly strained rings **71** and **72** consisting of a disilane linker and binaphthyl were synthesized.[115] The crystal structure revealed that the silicon atom is substantially deformed from the tetrahedral geometry. Take **71** as an example, the Si–Si–C(methyl) bond angle is enlarged to 119.0°. However, in the six-membered ring the Si–Si–C(naphthyl) bond angle is unusually restricted to 92.47°, which is significantly smaller than the idealized value of 109.5° for sp^3-hybridized silicon. The significant strain imposed by the reduced bond angle in the disilanylene moiety of **71** suggests that its Si–Si bond is highly reactive compared to that of other disilanylene-bridged compounds (**59–63**).

4. Applications

The unique conformational and electronic structure of a saturated Si–Si bridged σ–π hybrid endows compounds with functional properties. The typical application fields of disilane-bridged molecules include but are not limited to molecular electronics, nonlinear optics, AIE materials, CPL, electroluminescence, stimuli responsive materials, *etc*. In this section, we introduced the applications of the above mentioned aryldisilanes with emphasis on novel properties brought by silane linkages.

4.1. Electroluminescent materials

To achieve superior performance of organic emissive chromophores in OLEDs and other optical devices, addressing the issue of inadequate luminescence efficiency of dyes in the solid state is of utmost importance.[116] π-conjugated bipolar D–A molecular systems are widely employed as organic emitters; however, there are some drawbacks originating from the intrinsic molecular design. Usually, the donor and acceptor units are planar chromophores with large π systems, which are prone to aggregate in the solid state due to close intermolecular π–π interaction, resulting in lower fluorescence capacity. The electronic ground and excited states of the D–A structures are

energetically closer, which significantly increases the probability of internal conversion, owing to the higher probability of vibrational coupling. This makes it challenging to obtain organic fluorescent materials with high solid-state emission efficiency in the visible region. Meanwhile, the intramolecular charge transfer character of D–π–A architectures red-shifted the emission band and made the construction of pure blue and deep-blue luminophores a great challenge.[117]

For designing pure blue and deep blue organic electroluminescent materials, D–σ–A architectures have natural advantages.[75] Owing to the large atomic radius and tetrahedral conformation, organic Si–Si centered substituents are regarded as preferable bulky building blocks for the prevention of strong intermolecular π–π interaction. Their easy accessibility and chemical stability make it possible to install them on various sites of organic chromophores. The incorporation of Si substituents appropriately could manipulate the conformational and electronic properties of classic luminophores and liberate the emissive nature of the ones that are non-fluorescent in the solid state. Moreover, the bulky Si–Si substituents as π linkers would force the generation of twisted intramolecular charge transfer (TICT) in the D–A plane, which is beneficial for the design of highly emissive blue emitters.[118]

The quantum yields of D–σ–A–σ–D type compounds **37d–37f**, and **38d–38f** are low in DCM solution (Φ: 0.003–0.072).[86] However, their quantum yields in the solid state increased drastically (Φ: 0.040–0.247). Compound **38d** exhibits aggregation-induced emission enhancement (AIEE) properties. It emits sky-blue color in solution with a low quantum yield of 0.016, while the emission was enhanced in the solid state with a relatively high quantum yield of 0.247. Undoped LED devices using compound **38d** as the emitter exhibited green electroluminescence with an external quantum efficiency that reached a maximum of 0.65% (Fig. 8b). In addition, an OLED with **48**-doped dpVBi as an emissive layer was fabricated.[94] Tetrasila[2,2] cyclophanes possess high thermal stabilities and luminescence quantum yields in the solid state. This device showed blue-green luminescence at 495 nm with an external quantum efficiency of 0.36% on the preliminary study of electroluminescence indicating that tetrasila[2,2]cyclophanes are a good material for OLEDs.

4.2. Nonlinear optics

To create molecules belonging to the D–π–A class, organic π-systems can be capped using both an electron donor and an electron acceptor. The donor and acceptor units interact, leading to the formation of a low-energy π molecular orbital (MO) that spreads throughout the entire D–π–A system. In addition, the ICT induces polarization of the chromophore, resulting in a non-zero dipole moment.[119] The combination of these two features results in a non-zero first hyperpolarizability, which leads to a nonlinear response to the electric field of light. It is important to acknowledge that the transition from a molecular chromophore to a material necessitates further considerations, such as mechanical robustness, optical transparency, resistance to photodamage, and other criteria.
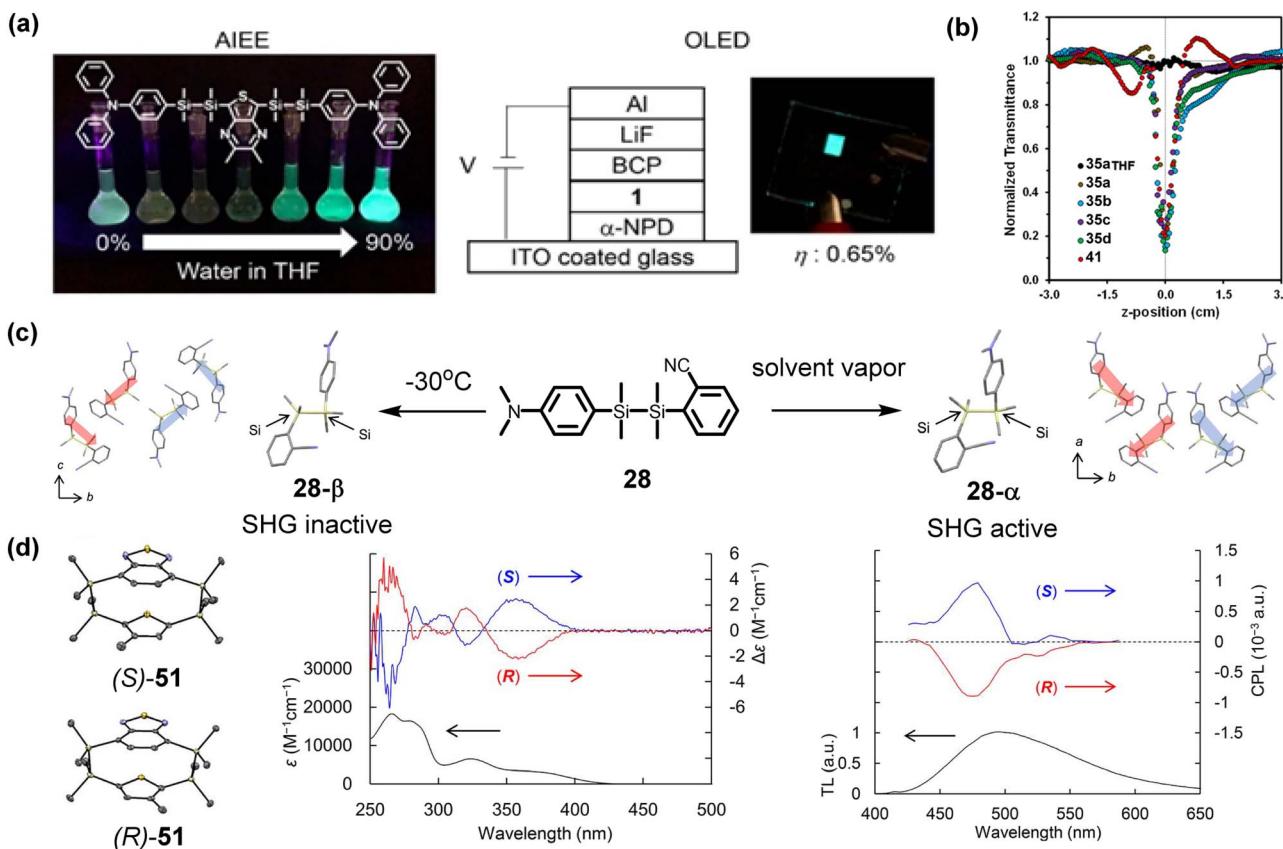
Fig. 8 (a) Application of **38d** in an electroluminescence device. Reproduced with permission from ref. 86, Copyright 2018, American Chemical Society. (b) Z-scan data of the PBC polymer thin films doped with **35** and **41**, respectively. Reproduced with permission from ref. 78, Copyright 2021, Royal Society of Chemistry. (c) The relationship of crystal packing and SHG activities of isomers of **28**. Reproduced with permission from ref. 120, Copyright 2020, American Chemical Society. (d) CPL performance of **51**. Reproduced with permission from ref. 94, Copyright 2017, American Chemical Society.

When a Si–Si σ bond is used to replace the π-conjugated linkage of a carbon-based D–A molecule, a D–σ–A molecule can be obtained. The Si–Si σ bridge serves to weaken, but not sever, the ICT between the donor and acceptor units. A D–σ–A system enables molecules with significant NLO responses while retaining the transparency of materials in the solution and solid state, since Si–Si σ conjugation and σ–π conjugation are much weaker for electron delocalization.

D–σ–A type disilane **28** was first reported to display solid-state second harmonic generation (SHG).[75] It possesses a significant transition dipole moment due to the presence of strong donor (–NMe$_2$) and acceptor (–CN) moieties connected by a Si–Si σ-conjugated linker. Molecules with extended π-conjugated structures usually exhibit strong absorption in the visible light region. In contrast, the Si–Si σ-conjugated molecules mentioned above do not show absorption in the visible light range. When exposed to Nd:YAG laser radiation ($\lambda = 1064$ nm), the compound exhibited a SHG efficiency that was 2.9 times greater than that of a urea crystal.

A subsequent investigation of compound **28** revealed an interesting phenomenon that this compound crystallized in two distinct polymorphic forms, **28-α** and **28-β**, under different crystallization conditions (Fig. 8c).[120] Distinct noncentrosymmetric (*Cc*; α-crystal) and centrosymmetric (*P*2$_1$/*c*; β-crystal) space groups were formed due to multiple CH–π interactions that resulted in different crystal packing arrangements. The noncentrosymmetric crystal **28-α** packing in a parallel manner exhibited SHG activity with an intensity 2.1 times higher than that of urea, while the antiparallel arrangement of centrosymmetric **28-β** showed no SHG activity. The control of SHG activity depends primarily on the crystal packing mode and orientation of the dipole moment. The modulation of SHG activity was achieved by controlling the formation of α- and β-crystals *via* phase transitions from supercooled liquid-to-crystal and crystal-to-crystal states.

Limiting the optical power, which is a major area of interest in nonlinear optics (NLO), is an effective method for safeguarding against high-intensity laser exposure. Disilane bridged D–σ–A architecture offers a possibility to fabricate multifunctional materials integrating solid-state emission, optical transparency, and NLO properties such as optical power limiting (OPL). The OPL properties of TPE based disilanes **35** and **41** doped on poly(bisphenol A carbonate) (PBC) thin films were investigated.[78] As expected for an optical power limiter, a powerful reverse saturable absorbance (RSA) response was detected, causing the normalized transmission rate to drop to

approximately 0.2 at the laser's focal point (Fig. 8b). Furthermore, the output fluence (I_{out}) attained a plateau as the input fluence increased. Due to the utilization of 7 ns laser pulses with a Gaussian laser pulse time profile, the observed RSA response may include contributions from excited state absorption originating from the S1 and/or T1 states, in addition to two-photon absorption, which would be dominant on a femtosecond timescale. The limiting threshold intensity (I_{lim}) values of 35 and 41 were estimated to be 2.6, 2.3, 3.0, 2.4 and 2.7 J cm^{-2}. None of the compounds displayed significant OPL properties when dissolved in THF, and there was no noticeable RSA response detected for the TPE-doped PBC thin film. Disilane-bridged structures have the potential to be ideal choices for creating organic–inorganic hybrid materials that exhibit a desirable balance between optical transparency and optical nonlinear properties in the solid state.

Due to their distinctive pull–push electronic properties and distorted structures, disilane-bridged BODIPYs **34** and **39** are likely to exhibit significant optical nonlinear properties. The largest two-photon absorption cross section (σ) determined by the open-aperture Z-scan method was 422990 GM for **34c**, which is superior to those of BODIPYs containing a carbon-based π-spacer (up to 10^3 GM) and comparable to those of porphyrin derivatives[121] (up to 6×10^5 GM) under identical measurement conditions.[122]

4.3. CPL materials

The value of the g_{lum} factor of small organic molecules for circularly polarized luminescence (CPL) tends to be relatively low (10^{-5} to 10^{-4}). Therefore, development on simple organic molecules showing a high g value is necessary for potential application in advanced materials. Since tetrasila[2,2]cyclophanes **51** containing a thiadiazole fragment are not racemized due to large steric hindrance, the optical resolution could be achieved with a chiral column.[94] **Rac-51** displays broad absorption with the maximum band at 370 nm and green luminescence at 490 nm. A mirror image of the circular dichroism spectra of **(S)-51** and **(R)-51** was observed with clear Cotton effects. In addition, the CPL spectra display opposite signals with g_{lum} values of 1.7×10^{-3} and 1.6×10^{-3} at 500 nm. The emission exhibited equivalent polarization in opposing directions, and the magnitudes were similar to those documented for molecules possessing helical and axial chirality. This skeleton can be further extended by structural modification and thus opens an avenue for the development of advanced chiroptical materials.

4.4. AIE and a dual-state emitter

Dual-state emissive (DSE) molecules are specifically designed substances that have the ability to emit strong fluorescence both in solution and in the solid state. These molecules are expected to have a diverse array of possible applications in various fields, such as energy, analytical chemistry, and molecular biology.[123] It is highly possible for organosilicon compounds to become dual-state emissive molecules due to the unique features of silicon.

In the disilane-bridged D–A–D and A–D–A molecular systems, the fluorescence quantum yields are primarily determined by the central aryl groups. Most compounds exhibit low quantum yields in dichloromethane (Φ: 0–0.10) due to the nonradiative relaxation caused by the molecular flexibility. However, most of their PLQYs in the solid state are higher than 0.20, indicating their AIE nature. Compound **37a** shows the highest quantum yield ($\Phi = 0.85$) in the solid state, and exhibits an obvious AIE effect in THF/H$_2$O mixtures (Fig. 9b). Compounds **73a**, **73b**, **74b**, **75a**, and **75b** are good DSE materials showing moderate quantum yields in both solution and the solid state. A–D–A molecule **75b** adopts an *anti*-formed straight crystal structure, and no intermolecular π–π interactions were found to inhibit the nonradiative transition. The HOMO and LUMO of **75b** were both localized on the bithiophene unit and Si–Si linkages, and its HOMO–LUMO transition represents the HOMO–LUMO π–π^* excitation. Consequently, the fluorescence of **75b** can be attributed to π^*–π transitions, which is different from the ICT emission of **73b** and **74b**. These results indicate that installing a disilane bridge between D–A moieties is an efficient design strategy for achieving highly fluorescent DSE materials.

In oligosilane-bridged bis-TPE compounds **14**,[26] the solid-state emission efficiency increased 1.6–2.8 times relative to that of TPE. The high lipid affinity of a silane chain makes it possible to use these silane-bridged compounds as latent fingerprint (LFP) development agents. Through simply dropping the CH$_3$CN/H$_2$O mixture of compounds on fingerprint surface, these bis-TPEs selectively adsorbed on the ridge of the
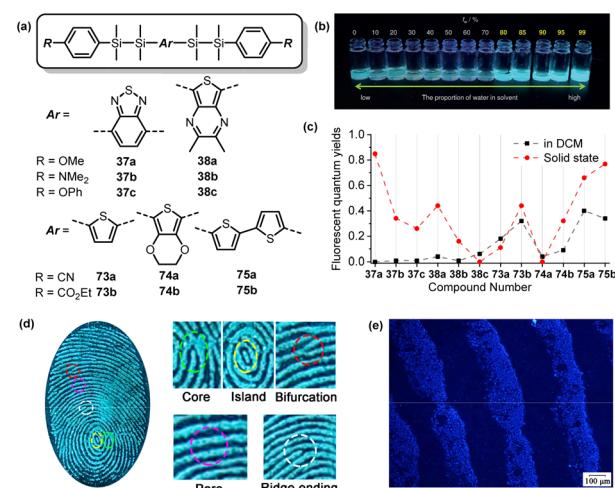

Fig. 9 (a) Chemical structures of DAD and ADA aryldisilanes. (b) Photographs of the photoluminescence of **38a** in various THF/water mixtures under 365 nm UV irradiation. Reproduced with permission from ref. 85, Copyright 2016, Wiley-VCH. (c) The absolute fluorescence quantum yields of compounds **37–38** and **73–75** in DCM solution and the solid state. The data in the figure are from ref. 85. (d) High-resolution photographic images of a LFP after treatment with **14** solution, showing level 1–3 details when excited with a 365 nm UV lamp. (e) False-color fluorescence image of the developed LFP showing adhesion of **14** aggregates to ridges. Reproduced with permission from ref. 26, Copyright 2020, Chinese Chemical Society.

fingerprint and emitted strongly. Level 1 to level 3 fingerprint information including the core, island, ridge ending, bifurcation, and even sweat-pore are clearly visualized (Fig. 9d). The fluorescence microscope images in Fig. 9b exhibit a conspicuous difference between the fluorescent ridges and nonfluorescent furrows, indicating that the compounds have a strong tendency to aggregate selectively at the fingerprint ridges.

4.5. Stimuli responsive materials

Materials that are stimuli-responsive have the ability to react to external stimuli, including but not limited to mechanical stress, heat, and exposure to solvents, in a reversible and highly sensitive manner. They promote fast advancements in biomedical and optoelectronics fields.[124] The flexibility and σ-electron delocalization of disilane bridges enable the control of stimuli-responsive behaviors of dyads and confer multifunctionality to materials.

Phenothiazine is a typical mechanochromic unit used in optoelectronic materials. In disilane-bridged compound **38g**,[87] the reversible fluorescence observed under external stimuli is mainly attributed to factors such as the packing mode in the crystalline state, conformational variation of phenothiazine, and the morphological differences between the crystalline and amorphous phases. In the solid state, compound **38g** exhibited a photoluminescence change that is both reversible and responsive to mechanical and thermal stimuli.[88] This can be explained by the intermolecular CH···π interaction, a relatively weak interaction that is prone to disruption and subsequent restoration in response to external stimuli. As shown in Fig. 10a, the conformer of **37g** and **38g** in the crystalline state facilitates the effective separation of the HOMO and LUMO between the phenothiazine donor and the thienopyrazine acceptor, which are connected by the disilane linker. Thus, the HOMO–LUMO energy transition is prohibited. The emission observed in the crystalline state corresponds to a LE state involving a LUMO → HOMO−1 transition. In the amorphous state, the presence of quasi-axial and quasi-equatorial conformers enables the transfer of energy from the predominant quasi-equatorial conformers, thereby facilitating ICT emission. The crystal packing of **37h** is mainly governed by weak CH···π interactions, which are weak interactions that can be easily disrupted and reformed under external stimuli, leading to the observed dual emission. In contrast, **37i** displayed strong π–π interaction between two phenoxazine moieties in its crystalline packing. Furthermore, the (pseudo)planar structure of phenoxazine precludes the presence of conformers such as quasi-axial and quasi-equatorial isomers.

Soft crystals are characterized by a single crystal-to-single-crystal (SCSC) transition that occurs in response to heat, light, or pressure.[28] External stimuli can induce changes in the conformational, mechanical, photophysical, and electrochemical performances of soft crystals, thereby enabling tuning and switching of their functionalities. Recently, Nishihara's research group prepared disilanyl macrocycle **76** consisting of four *p*-phenylenes connected in a circular manner *via* four flexible disilane bonds.[125] Although this structure was
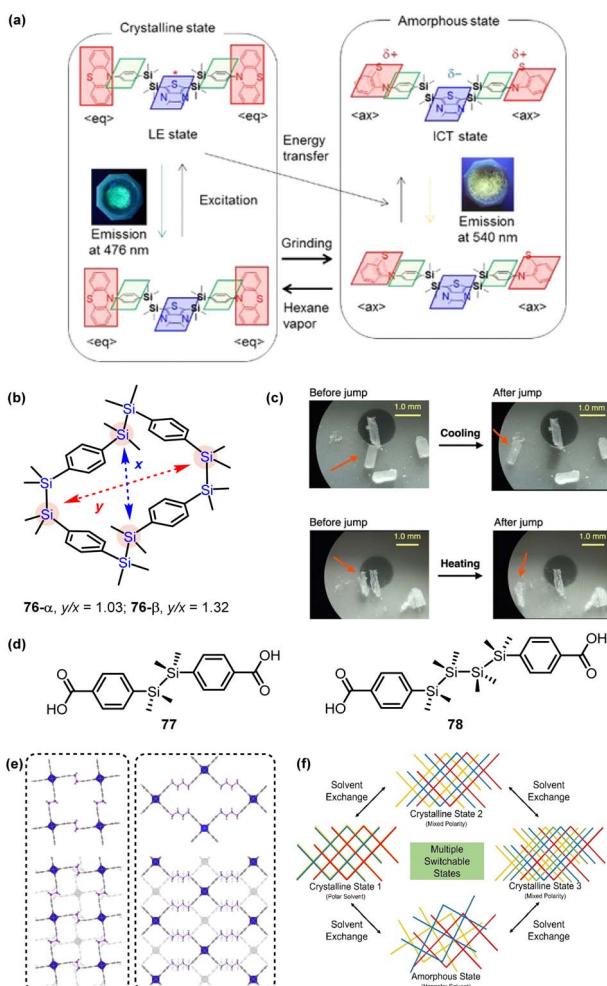

Fig. 10 (a) Plausible mechanism for fluorescence in crystalline and amorphous states of **38g**. Reproduced with permission from ref. 87, Copyright 2021, Wiley-VCH. (b) The structural difference between the two isomers of **76**. (c) Microscopy images show the thermosalient effect of **76-α** or **76-β** undergoing (up) cooling and (down) heating processes between 30 and -196 °C. The crystals that exhibit the thermosalient effect are highlighted using red arrows. Reproduced with permission from ref. 125, Copyright 2020, American Chemical Society. (d) Structures of disilane and tetrasilane bridged ligands **77** and **78**. (e) Monolayer segments and view of sheet stacking as seen down the stacking direction for the **77-Cu** MOF (left) and **78-Cu** MOF (right). (f) **77-Cu** and **78-Cu** MOFs are composed of 2D sheets with solvent-dependent stacking arrangements. Reproduced with permission from ref. 126, Copyright 2020, Wiley-VCH.

synthesized 30 years ago by an alternative method, photophysical and conformational studies other than UV spectral analysis were scarcely reported.[91] Thorough investigation of the aged compound led to a novel discovery. Single crystals of **76** exhibited a reversible thermal SCSC phase transition between two crystal phases **76-α** and **76-β** induced by cooling and heating. Interestingly, remarkable mechanical motion accompanied with SCSC (thermosalient effect) was observed. The flexibility of the parallelogram-shaped disilanyl architecture was evidenced by the varying y/x ratio observed in different crystals (Fig. 10b). The collective structural transformation of the macrocycles in

the crystal (known as a parallel crank motion) was facilitated by the packing mode of the molecules, which relies on relatively weak intermolecular interactions. This transformation led to a SCSC phase transition, accompanied by anisotropic shrinking/elongation of the cells, ultimately resulting in the thermosalient effect.

Another example of using an oligosilane chain to construct "soft crystal" smart materials was reported recently. Novel MOFs that respond to chemical stimuli were synthesized using Cu paddlewheel nodes and disilane and tetrasilane linkers 77 and 78.[126] They possess the unique ability to attain multiple crystalline and amorphous states. The stacking arrangement of the layers in the 2D MOF networks is determined by the identity and polarity of the solvent trapped within. By manipulating the solvent through exchange, the crystalline state can be reversibly transformed between various crystalline and amorphous phases (Fig. 10f). Under thermal activation, these MOFs are capable of undergoing additional structural transformations. The increased flexibility of the four silicon chains in the **78-Cu** MOF makes its phase transition more energetically favorable, allowing the MOF to transition more rapidly and achieve a more stable configuration.

5. Conclusions

Over the past decade, σ-conjugated systems with disilane bridges have emerged as a versatile class of materials for molecular electronics and optoelectronics. σ-π hybrid architectures combine organic conjugated molecules with organosilicon units, resulting in novel physical and chemical functionalities that are hardly achieved using π-conjugated systems. The introduction of disilane linkages into π-conjugated units can regulate the optoelectronic properties due to the following features: (1) σ-electron delocalization along the Si–Si bond; (2) comparable HOMO energy with most π systems and the resulting σ–π conjugation effect; (3) electron-donating ability caused by low ionization energy; (4) the bulkiness and flexibility of a saturated Si–Si unit. As a result, disilane-bridged σ-conjugated systems exhibit several unique properties that are not always present in π-conjugated systems. Disilane bridged σ-conjugated molecules are usually highly emissive in the solid state, and are optically transparent; they are widely used in photoluminescence materials, electroluminescence devices, NLO, AIE, CPL, and stimuli-responsive materials.

Thanks to the continuous development of the C–Si bond construction method, the above-mentioned molecules with unique properties can be synthesized and used to study structure–performance relationships. Linear disilanes and macrocyclic molecules with distinctive structures can be obtained. The rational selection of end-capped chromophores and connection manner of disilanes have proved to be key factors for regulating material functions.

In the future, disilane-bridged D–σ–A systems are likely to continue to gain research interest in the fields of multifunctional optoelectronics, especially smart materials. Many structurally impressive disilane bridged compounds have been reported in the past few decades. Unfortunately, research on physical and chemical properties other than absorption and fluorescence is still relatively superficial and highly worthy of being further explored. This is an important research area in disilane-bridged architectures, just as the saying goes, "An old tree can still sprout new flowers." In addition, synthetic methods still need continuous innovation since the structural diversity of D–σ–A molecules is still insufficient for fundamental and applied research. Although the transition metal catalyzed mono Si–C bond-forming reaction has been extensively explored, novel catalytic reactions for constructing Si–Si–C bonds are rare since the Si–Si bond is easily broken in transition metal-catalyzed reactions. During the Pd(0)-catalyzed Si–Si–C coupling reaction, we can still observe the breaking of Si–Si bonds.[127] Moreover, longer silane chain (more than two Si atoms) bridged D–σ–A molecules are essentially unexplored. Recent studies have shown that the electrochemical method based on chlorosilanes as raw materials has the potential to become a mild and universal new pathway for Si–C coupling.[48] Hence, through synthetic chemistry innovation, disilane-bridged architectures would find more applications in practice and behave even better than their π linker-bridged molecular counterparts in certain aspects.

Author contributions

Z. Z. and H. L. conceived the idea. Z. Z., H. L., L. G., L. W. X. and Z. G. contributed to the writing, review and editing of the manuscript. All authors have given approval to the final version of the manuscript.

Conflicts of interest

There are no conflicts to declare.

Acknowledgements

References

1 R. D. Miller and J. Michl, *Chem. Rev.*, 1989, **89**, 1359–1410.

2 H. K. Sharma and K. H. Pannell, *Chem. Rev.*, 1995, **95**, 1351–1374.

3 Y. Zuo, X. Liang, J. Yin, Z. Gou and W. Lin, *Coord. Chem. Rev.*, 2021, **447**, 214166.

4 H. Wang, X. Zhang, Y. Li and L.-W. Xu, *Angew. Chem., Int. Ed.*, 2022, **61**, e202210851.

5 H. Shi, J. Yang, Z. Li and C. He, *Silicon Containing Hybrid Copolym.*, 2020, 1–21, DOI: **10.1002/9783527823499.ch1**.

6 H. Wang, S. Chen, Y. Li, Y. Liu, Q. Jing, X. Liu, Z. Liu and X. Zhang, *Adv. Energy Mater.*, 2021, **11**, 2101057.

7 M. C. Kung, M. V. Riofski, M. N. Missaghi and H. H. Kung, *Chem. Commun.*, 2014, **50**, 3262–3276.

8 S. P. Koiry and A. K. Chauhan, in *Handbook on Synthesis Strategies for Advanced Materials: Volume-III: Materials Specific Synthesis Strategies*, ed. A. K. Tyagi and R. S. Ningthoujam, Springer Singapore, Singapore, 2021, pp. 831–866, DOI: 10.1007/978-981-16-1892-5_17.

9 M. Akhtaruzzaman, Y. Seya, N. Asao, A. Islam, E. Kwon, A. El-Shafei, L. Han and Y. Yamamoto, *J. Mater. Chem.*, 2012, **22**, 10771–10778.

10 K. L. Chan, M. J. McKiernan, C. R. Towns and A. B. Holmes, *J. Am. Chem. Soc.*, 2005, **127**, 7662–7663.

11 J. Luo, Z. Xie, J. W. Y. Lam, L. Cheng, H. Chen, C. Qiu, H. S. Kwok, X. Zhan, Y. Liu, D. Zhu and B. Z. Tang, *Chem. Commun.*, 2001, 1740–1741.

12 X. Xiang, Z. Zhou, X. Wu, Z. Ni, L. Gai, X. Xiao, L. Xu, Z. Zhao, H. Lu and Z. Guo, *CCS Chem.*, 2022, **4**, 3798–3808.

13 R.-H. Tang, Z. Xu, Y.-X. Nie, X.-Q. Xiao, K.-F. Yang, J.-L. Xie, B. Guo, G.-W. Yin, X.-M. Yang and L.-W. Xu, *iScience*, 2020, **23**, 101268.

14 T. Karatsu, *J. Photochem. Photobiol., C*, 2008, **9**, 111–137.

15 Y. Zhang, X.-C. Wang, C.-W. Ju and D. Zhao, *Nat. Commun.*, 2021, **12**, 68.

16 P. Xiao, L. Gao and Z. Song, *Chem.–Eur. J.*, 2019, **25**, 2407–2422.

17 I. Beletskaya and C. Moberg, *Chem. Rev.*, 2006, **106**, 2320–2354.

18 K. A. Horn, *Chem. Rev.*, 1995, **95**, 1317–1350.

19 V. Pophristic, L. Goodman and C. T. Wu, *J. Phys. Chem. A*, 2001, **105**, 7454–7459.

20 R. G. Kepler, *Synth. Met.*, 1989, **28**, 573–580.

21 H. A. Fogarty, D. L. Casher, R. Imhof, T. Schepers, D. W. Rooklin and J. Michl, *Pure Appl. Chem.*, 2003, **75**, 999.

22 R. S. Klausen, J. R. Widawsky, M. L. Steigerwald, L. Venkataraman and C. Nuckolls, *J. Am. Chem. Soc.*, 2012, **134**, 4541–4544.

23 J. V. Ortiz, *J. Chem. Phys.*, 1991, **94**, 6064–6072.

24 H. Sakurai, *Pure Appl. Chem.*, 1987, **59**, 1637–1646.

25 M. Kira, T. Miyazawa, H. Sugiyama, M. Yamaguchi and H. Sakurai, *J. Am. Chem. Soc.*, 1993, **115**, 3116–3124.

26 X. Xiang, Z. Zhou, H. Feng, S. Feng, L. Gai, H. Lu and Z. Guo, *CCS Chem.*, 2020, **2**, 329–336.

27 S. Hirata, M. Nishio, H. Uchida, T. Usuki, T. Nakae, M. Miyachi, Y. Yamanoi and H. Nishihara, *J. Phys. Chem. C*, 2020, **124**, 3277–3286.

28 M. Kato, H. Ito, M. Hasegawa and K. Ishii, *Chem.–Eur. J.*, 2019, **25**, 5105–5112.

29 A. K. Franz and S. O. Wilson, *J. Med. Chem.*, 2013, **56**, 388–405.

30 T. A. Su, H. Li, R. S. Klausen, N. T. Kim, M. Neupane, J. L. Leighton, M. L. Steigerwald, L. Venkataraman and C. Nuckolls, *Acc. Chem. Res.*, 2017, **50**, 1088–1095.

31 F. S. Kipping and J. E. Sands, *J. Chem. Soc., Trans.*, 1921, **119**, 830–847.

32 T. D. Tilley, *Acc. Chem. Res.*, 1993, **26**, 22–29.

33 L. Chen, J.-B. Huang, Z. Xu, Z.-J. Zheng, K.-F. Yang, Y.-M. Cui, J. Cao and L.-W. Xu, *RSC Adv.*, 2016, **6**, 67113–67117.

34 M. Murata, K. Suzuki, S. Watanabe and Y. Masuda, *J. Org. Chem.*, 1997, **62**, 8569–8571.

35 A. S. Manoso and P. DeShong, *J. Org. Chem.*, 2001, **66**, 7449–7455.

36 Y. Yamanoi, *J. Org. Chem.*, 2005, **70**, 9607–9609.

37 A. Lesbani, H. Kondo, Y. Yabusaki, M. Nakai, Y. Yamanoi and H. Nishihara, *Chem.–Eur. J.*, 2010, **16**, 13519–13527.

38 A. A. Toutov, W.-B. Liu, K. N. Betz, A. Fedorov, B. M. Stoltz and R. H. Grubbs, *Nature*, 2015, **518**, 80–84.

39 J. V. Obligacion and P. J. Chirik, *Nat. Rev. Chem*, 2018, **2**, 15–34.

40 C. Cheng and J. F. Hartwig, *Science*, 2014, **343**, 853–857.

41 C. Cheng and J. F. Hartwig, *Chem. Rev.*, 2015, **115**, 8946–8975.

42 S. C. Richter and M. Oestreich, *Trends Chem.*, 2020, **2**, 13–27.

43 U. Schubert, *Angew Chem. Int. Ed. Engl.*, 1994, **33**, 419–421.

44 M. Suginome and Y. Ito, *J. Chem. Soc., Dalton Trans.*, 1998, 1925–1934.

45 A. Lesbani, H. Kondo, J.-i. Sato, Y. Yamanoi and H. Nishihara, *Chem. Commun.*, 2010, **46**, 7784–7786.

46 Y. Kimata, H. Suzuki, S. Satoh and A. Kuriyama, *Organometallics*, 1995, **14**, 2506–2511.

47 A. D. Beck, S. Haufe, J. Tillmann and S. R. Waldvogel, *ChemElectroChem*, 2022, **9**, e202101374.

48 W. Guan, L. Lu, Q. Jiang, A. F. Gittens, Y. Wang, L. F. T. Novaes, R. S. Klausen and S. Lin, *Angew. Chem., Int. Ed.*, 2023, **62**, e202303592.

49 A. Bande and J. Michl, *Chem.–Eur. J.*, 2009, **15**, 8504–8517.

50 H. Gilman, W. H. Atwell and G. L. Schwebke, *J. Organomet. Chem.*, 1964, **2**, 369–371.

51 T. Hayato, S. Yuki, T. Tohru, K. Makoto and T. Kohei, *Bull. Chem. Soc. Jpn.*, 2005, **78**, 1334–1344.

52 J. Michl and R. West, *Acc. Chem. Res.*, 2000, **33**, 821–823.

53 A. Fukazawa, H. Tsuji and K. Tamao, *J. Am. Chem. Soc.*, 2006, **128**, 6800–6801.

54 M. Linnemannstöns, J. Schwabedissen, B. Neumann, H.-G. Stammler, R. J. F. Berger and N. W. Mitzel, *Chem.–Eur. J.*, 2020, **26**, 2169–2173.

55 T. Karatsu, T. Shibata, A. Nishigaki, A. Kitamura, Y. Hatanaka, Y. Nishimura, S.-i. Sato and I. Yamazaki, *J. Phys. Chem. B*, 2003, **107**, 12184–12191.

56 D.-D. H. Yang, N.-c. C. Yang, I. M. Steele, H. Li, Y.-Z. Ma and G. R. Fleming, *J. Am. Chem. Soc.*, 2003, **125**, 5107–5110.

57 K. V. Zaitsev, K. Lam, O. K. Poleshchuk, L. G. Kuz'mina and A. V. Churakov, *Dalton Trans.*, 2018, **47**, 5431–5444.

58 A. Hameau, F. Guyon, M. Knorr, C. Däschlein, C. Strohmann and N. Avarvari, *Dalton Trans.*, 2008, 4866–4876.

59 S. C. Jones, S. Barlow and D. O'Hare, *Chem.–Eur. J.*, 2005, **11**, 4473–4481.

60 V. V. Dement'ev, F. Cervantes-Lee, L. Parkanyi, H. Sharma, K. H. Pannell, M. T. Nguyen and A. Diaz, *Organometallics*, 1993, **12**, 1983–1987.

61 S. Feng, Z. Zhou, X. Xiang, H. Feng, Z. Qu and H. Lu, *ACS Omega*, 2020, **5**, 19181–19186.

62 M. Shimizu and T. Sakurai, *Aggregate*, 2022, **3**, e144.

63 C. Zhou, Z. Zhou, F. Yu, W. Xie, W. Zhang, Q. Yang, X. Xu, L. Gai and H. Lu, *J. Mater. Chem. C*, 2022, **10**, 18182–18188.

64 S. Surampudi, M. L. Yeh, M. A. Siegler, J. F. M. Hardigree, T. A. Kasl, H. E. Katz and R. S. Klausen, *Chem. Sci.*, 2015, **6**, 1905–1909.

65 C. Marschner, J. Baumgartner and A. Wallner, *Dalton Trans.*, 2006, 5667–5674.

66 J. Zhou, C. P. Folster, S. K. Surampudi, D. Jimenez, R. S. Klausen and A. E. Bragg, *Dalton Trans.*, 2017, **46**, 8716–8726.

67 B. J. Barrett, D. Jimenez, R. S. Klausen and A. E. Bragg, *J. Phys. Chem. B*, 2021, **125**, 8460–8471.

68 M. Tanabe, R. Yumoto and K. Osakada, *Chem. Commun.*, 2012, **48**, 2125–2127.

69 M. Tanabe, R. Yumoto, K. Osakada, T. Sanji and M. Tanaka, *Organometallics*, 2012, **31**, 6787–6795.

70 V. E. M. Kaats-Richters, T. J. Cleij, L. W. Jenneskens, M. Lutz, A. L. Spek and C. A. van Walree, *Organometallics*, 2003, **22**, 2249–2258.

71 C. P. Folster, P. N. Nguyen, M. A. Siegler and R. S. Klausen, *Organometallics*, 2019, **38**, 2902–2909.

72 G. Mignani, M. Barzoukas, J. Zyss, G. Soula, F. Balegroune, D. Grandjean and D. Josse, *Organometallics*, 1991, **10**, 3660–3668.

73 G. Mignani, A. Kramer, G. Puccetti, I. Ledoux, G. Soula, J. Zyss and R. Meyrueix, *Organometallics*, 1990, **9**, 2640–2643.

74 G. Mignani, A. Kramer, G. Puccetti, I. Ledoux, J. Zyss and G. Soula, *Organometallics*, 1991, **10**, 3656–3659.

75 M. Shimada, Y. Yamanoi, T. Matsushita, T. Kondo, E. Nishibori, A. Hatakeyama, K. Sugimoto and H. Nishihara, *J. Am. Chem. Soc.*, 2015, **137**, 1024–1027.

76 H. K. Sharma, K. H. Pannell, I. Ledoux, J. Zyss, A. Ceccanti and P. Zanello, *Organometallics*, 2000, **19**, 770–774.

77 X. Zheng, W. Du, L. Gai, X. Xiao, Z. Li, L. Xu, Y. Tian, M. Kira and H. Lu, *Chem. Commun.*, 2018, **54**, 8834–8837.

78 H. Feng, Z. Zhou, A. K. May, J. Chen, J. Mack, T. Nyokong, L. Gai and H. Lu, *J. Mater. Chem. C*, 2021, **9**, 6470–6476.

79 A. A. Strelnikov, A. S. Konev, O. V. Levin, A. F. Khlebnikov, A. Iwasaki, K. Yamanouchi and N. V. Tkachenko, *J. Phys. Chem. B*, 2020, **124**, 10899–10912.

80 H. Imahori and S. Fukuzumi, *Adv. Funct. Mater.*, 2004, **14**, 525–536.

81 M. Sasaki, Y. Shibano, H. Tsuji, Y. Araki, K. Tamao and O. Ito, *J. Phys. Chem. A*, 2007, **111**, 2973–2979.

82 Y. Kobori, Y. Shibano, T. Endo, H. Tsuji, H. Murai and K. Tamao, *J. Am. Chem. Soc.*, 2009, **131**, 1624–1625.

83 Y. Kobori, M. Fuki and H. Murai, *J. Phys. Chem. B*, 2010, **114**, 14621–14630.

84 Y. Shibano, M. Sasaki, H. Tsuji, Y. Araki, O. Ito and K. Tamao, *J. Organomet. Chem.*, 2007, **692**, 356–367.

85 M. Shimada, M. Tsuchiya, R. Sakamoto, Y. Yamanoi, E. Nishibori, K. Sugimoto and H. Nishihara, *Angew. Chem., Int. Ed.*, 2016, **55**, 3022–3026.

86 T. Usuki, M. Shimada, Y. Yamanoi, T. Ohto, H. Tada, H. Kasai, E. Nishibori and H. Nishihara, *ACS Appl. Mater. Interfaces*, 2018, **10**, 12164–12172.

87 T. Nakae, M. Nishio, T. Usuki, M. Ikeya, C. Nishimoto, S. Ito, H. Nishihara, M. Hattori, S. Hayashi, T. Yamada and Y. Yamanoi, *Angew. Chem., Int. Ed.*, 2021, **60**, 22871–22878.

88 H. Miyabe, M. Ujita, M. Nishio, T. Nakae, T. Usuki, M. Ikeya, C. Nishimoto, S. Ito, M. Hattori, S. Takeya, S. Hayashi, D. Saito, M. Kato, H. Nishihara, T. Yamada and Y. Yamanoi, *J. Org. Chem.*, 2022, **87**, 8928–8938.

89 C. J. Brown and A. C. Farthing, *Nature*, 1949, **164**, 915–916.

90 Z. Hassan, E. Spuling, D. M. Knoll and S. Bräse, *Angew. Chem., Int. Ed.*, 2020, **59**, 2156–2170.

91 H. Sakurai, *Adv. Inorg. Chem.*, 2000, **50**, 359–407.

92 S. Hideki, H. Satoshi, K. Akihiko, H. Akira and K. Chizuko, *Chem. Lett.*, 1986, **15**, 1781–1784.

93 M. Kira and S. Tokura, *Organometallics*, 1997, **16**, 1100–1102.

94 M. Shimada, Y. Yamanoi, T. Ohto, S.-T. Pham, R. Yamada, H. Tada, K. Omoto, S. Tashiro, M. Shionoya, M. Hattori, K. Jimura, S. Hayashi, H. Koike, M. Iwamura, K. Nozaki and H. Nishihara, *J. Am. Chem. Soc.*, 2017, **139**, 11214–11221.

95 W. Nakanishi, S. Hitosugi, A. Piskareva, Y. Shimada, H. Taka, H. Kita and H. Isobe, *Angew. Chem., Int. Ed.*, 2010, **49**, 7239–7242.

96 W. Nakanishi, S. Hitosugi, Y. Shimada and H. Isobe, *Chem.–Asian J.*, 2011, **6**, 554–559.

97 W. Nakanishi, Y. Shimada, H. Taka, H. Kita and H. Isobe, *Org. Lett.*, 2012, **14**, 1636–1639.

98 W. Nakanishi, Y. Shimada and H. Isobe, *Chem.–Asian J.*, 2013, **8**, 1177–1181.

99 W. Nakanishi, N. Matsuyama, D. Hara, A. Saeki, S. Hitosugi, S. Seki and H. Isobe, *Chem.–Asian J.*, 2014, **9**, 1782–1785.

100 K. Kato, K. Fujimoto, H. Yorimitsu and A. Osuka, *Chem.–Eur. J.*, 2015, **21**, 13522–13525.

101 J. B. Gilroy, A. D. Russell, A. J. Stonor, L. Chabanne, S. Baljak, M. F. Haddow and I. Manners, *Chem. Sci.*, 2012, **3**, 830–841.

102 W. Finckh, B. Z. Tang, A. Lough and I. Manners, *Organometallics*, 1992, **11**, 2904–2911.

103 M. Kumada, T. Kondo, K. Mimura, M. Ishikawa, K. Yamamoto, S. Ikeda and M. Kondo, *J. Organomet. Chem.*, 1972, **43**, 293–305.

104 H. Wagner, J. Baumgartner and C. Marschner, *Organometallics*, 2007, **26**, 1762–1770.

105 H. Braunschweig, A. Damme, K. Hammond and J. Mager, *Organometallics*, 2012, **31**, 6317–6321.

106 H. Braunschweig, F. Breher, M. Kaupp, M. Gross, T. Kupfer, D. Nied, K. Radacki and S. Schinzel, *Organometallics*, 2008, **27**, 6427–6433.

107 H. Braunschweig and T. Kupfer, *Organometallics*, 2007, **26**, 4634–4638.

108 F. M. de Rege, J. D. Kassebaum, B. L. Scott, K. D. Abney and G. J. Balaich, *Inorg. Chem.*, 1999, **38**, 486–489.

109 J. Ohshita, Y. Adachi, D. Tanaka, M. Nakashima and Y. Ooyama, *RSC Adv.*, 2015, **5**, 36673–36679.

110 J. Ohshita, M. Nodono, H. Kai, T. Watanabe, A. Kunai, K. Komaguchi, M. Shiotani, A. Adachi, K. Okita,

Y. Harima, K. Yamashita and M. Ishikawa, *Organometallics*, 1999, **18**, 1453–1459.

111 M. Shimizu, H. Tatsumi, K. Mochida, K. Oda and T. Hiyama, *Chem.–Asian J.*, 2008, **3**, 1238–1247.

112 M. Oba, M. Iida, T. Nagoya and K. Nishiyama, *J. Organomet. Chem.*, 2006, **691**, 1151–1153.

113 J. Ohshita, T. Kai, Y. Adachi, K. Yamaji, M. Nakamura, S. Watase, S. Mori and N. Matsuyama, *Appl. Organomet. Chem.*, 2020, **34**, e5306.

114 T. Nakae, H. Miyabe, M. Nishio, T. Yamada and Y. Yamanoi, *Molecules*, 2021, **26**, 6852.

115 T. Hoshi, T. Nakamura, T. Suzuki, M. Ando and H. Hagiwara, *Organometallics*, 2000, **19**, 3170–3178.

116 Y. Li, T. Liu, H. Liu, M.-Z. Tian and Y. Li, *Acc. Chem. Res.*, 2014, **47**, 1186–1198.

117 J. Yang, J. Huang, Q. Li and Z. Li, *J. Mater. Chem. C*, 2016, **4**, 2663–2684.

118 Y. Zheng, Z. Wang, X. Wang, J. Li, X. J. Feng, G. He, Z. Zhao and H. Lu, *ACS Appl. Electron. Mater.*, 2021, **3**, 422–429.

119 R. Misra and S. P. Bhattacharyya, in *Intramolecular Charge Transfer*, John Wiley & Sons, 2018, ch. 5, pp. 149–195, DOI: **10.1002/9783527801916.ch5**.

120 M. Nishio, M. Shimada, K. Omoto, T. Nakae, H. Maeda, M. Miyachi, Y. Yamanoi, E. Nishibori, N. Nakayama, H. Goto, T. Matsushita, T. Kondo, M. Hattori, K. Jimura, S. Hayashi and H. Nishihara, *J. Phys. Chem. C*, 2020, **124**, 17450–17458.

121 H. Rath, J. Sankar, V. PrabhuRaja, T. K. Chandrashekar, A. Nag and D. Goswami, *J. Am. Chem. Soc.*, 2005, **127**, 11608–11609.

122 B. Kim, X. Yue, B. Sui, X. Zhang, Y. Xiao, M. V. Bondar, J. Sawada, M. Komatsu and K. D. Belfield, *Eur. J. Org Chem.*, 2015, **2015**, 5563–5571.

123 J. L. Belmonte-Vázquez, Y. A. Amador-Sánchez, L. A. Rodríguez-Cortés and B. Rodríguez-Molina, *Chem. Mater.*, 2021, **33**, 7160–7184.

124 S. K. Mellerup and S. Wang, *Chem. Soc. Rev.*, 2019, **48**, 3537–3549.

125 K. Omoto, T. Nakae, M. Nishio, Y. Yamanoi, H. Kasai, E. Nishibori, T. Mashimo, T. Seki, H. Ito, K. Nakamura, N. Kobayashi, N. Nakayama, H. Goto and H. Nishihara, *J. Am. Chem. Soc.*, 2020, **142**, 12651–12657.

126 D. A. Burns, E. M. Press, M. A. Siegler, R. S. Klausen and V. S. Thoi, *Angew. Chem., Int. Ed.*, 2020, **59**, 763–768.

127 S. Wang, H. Lu, Y. Wu, X. Xiao, Z. Li, M. Kira and Z. Shen, *Chem.–Asian J.*, 2017, **12**, 561–567.